Plant Physiology Preview. Published on November 14, 2017, as DOI:10.1104/pp.17.01545

Short title: Role of RH50 in plastid rRNA maturation and signaling

Corresponding author details:

Dario Leister
Ludwig-Maximilians-University Munich
Department Biology I
Großhaderner Str. 2
D-82152 Planegg-Martinsried
Germany
Phone: +49-89/2180 74550
Fax: +49-89/2180 74599
E-mail: leister@lmu.de

The DEAD-box RNA helicase RH50 is a 23S-4.5S rRNA maturation factor that functionally overlaps with the plastid signaling factor GUN1[1]

Francesca Paieri[2], Luca Tadini[2], Nikolay Manavski[2], Tatjana Kleine, Roberto Ferrari, Piero Morandini, Paolo Pesaresi, Jörg Meurer and Dario Leister[*]

Faculty of Biology, Ludwig-Maximilians-Universität München, D-82152 Planegg-Martinsried, Germany (FP, LT, NM, TK, JM, DL); Centro Ricerca e Innovazione, Fondazione Edmund Mach, I-38010, San Michele all'Adige, Italy (FP); Department of Biosciences (RF, PM) and Department of Agricultural and Environmental Sciences - Production, Landscape, Agroenergy (PP), I-20133 Milano, Italy (PP)

One-sentence summary: RH50 is required for processing of chloroplast ribosomal RNA and shares several features with the signaling factor GUN1, including intrachloroplast localization, expression profile, and epistatic effects.

List of author contributions:

D.L. conceived the research plan; J.M., P.P. and D.L. supervised the experiments; F.P., L.T., N.M., T.K., R.F. and P.M. performed and analyzed the experiments; F.P. wrote the manuscript with contributions from all authors; D.L. supervised the writing process and prepared the final version.

[1] This work was supported by the Deutsche Forschungsgemeinschaft (TRR 175, projects A03, C01 and C05)

[2] These authors contributed equally to the article

* Address correspondence to leister@lmu.de

ABSTRACT

DEAD-box RNA helicases (DBRHs) modulate RNA secondary structure, allowing RNA molecules to adopt the conformations required for interaction with their target proteins. RH50 is a chloroplast-located DBRH that co-localizes and is co-expressed with GUN1, a central factor in chloroplast-to-nucleus signaling. When combined with mutations that impair plastid gene expression (*prors1-1*, *prpl11-1*, *prps1-1*, *prps21-1*, *prps17-1* and *prpl24-1*), *rh50* and *gun1* mutations evoke similar patterns of epistatic effects. These observations, together with the synergistic growth phenotype of the double mutant *rh50-1 gun1-102*, suggest that RH50 and GUN1 are functionally related and that this function is associated with plastid gene expression, in particular ribosome functioning. However, *rh50-1* itself is not a gun mutant, although - like *gun1-102* – the *rh50-1* mutation suppresses the down-regulation of nuclear genes for photosynthesis induced by the *prors1-1* mutation. The RH50 protein co-migrates with ribosomal particles, and is required for efficient translation of plastid proteins. RH50 binds to transcripts of the 23S-4.5S intergenic region and, in its absence, levels of the corresponding rRNA processing intermediate are strongly increased, implying that RH50 is required for the maturation of the 23S and 4.5S rRNAs. This inference is supported by the finding that loss of RH50 renders chloroplast protein synthesis sensitive to erythromycin and exposure to cold. Based on these results, we conclude that RH50 is a plastid rRNA maturation factor.

67

68

INTRODUCTION

DEAD-box RNA helicases (DBRHs) contain at least nine conserved motifs that constitute the helicase core domain, including the stretch of highly conserved Asp-Glu-Ala-Asp (D-E-A-D) residues in motif II that gave this protein family its name (Caruthers and McKay, 2002; Cordin et al., 2006). DBRHs participate in many cellular processes, including RNA metabolism (synthesis, modification, cleavage and degradation), ribosome biogenesis and translation initiation (Silverman et al., 2003; Cordin et al., 2006). RNA molecules must fold into specific conformations in order to interact with proteins, and DBRHs facilitate the remodeling of RNA secondary structure by unwinding duplexes in a localized strand separation reaction (Jarmoskaite and Russell, 2011). To this end, the helicase binds to the duplex region, interacts with one end of the duplex and then uses energy from cycles of ATP binding and hydrolysis to translocate directionally along one of the strands while displacing the other (Jarmoskaite and Russell, 2011). Recent data suggest that DBRHs have distinct activities compared to other superfamily 2 (SF2) RNA helicase proteins, and often do not show the same unwinding activity as observed for other SF2 RNA helicases (Jarmoskaite and Russell, 2014).

In all, 58 DBRHs have been annotated in the *Arabidopsis thaliana* genome (Mingam et al., 2004), ten of which (RH3, 11, 17, 22, 26, 33, 41, 50, 52, 58) are predicted to be plastid-localized (Asakura et al., 2012). Mass spectrometry analyses have meanwhile confirmed the presence of seven DBRHs in *A. thaliana* chloroplasts, namely RH3, 22, 26, 39, 47, 50 and 58 (Olinares et al., 2010; Majeran et al., 2012). Phylogenetic analyses cluster the plastid DBRHs into several groups: RH3 is assigned to a subset with mitochondrial and nuclear orthologs; RH26 belongs to a clade containing proteins of unknown function, whereas RH22, RH39, RH47, RH50 and RH58 form a separate group (Asakura et al., 2012; Chi et al., 2012). Some of the plastid helicases have been functionally characterized. The *rh39* mutant accumulates

precursors of the 23S rRNA, indicating that RH39 is involved in plastid rRNA maturation, and is required to introduce the hidden break into the 23S rRNA (Nishimura et al., 2010). RH22 is also involved in the assembly of the 50S ribosomal subunit in the chloroplast: complete loss of RH22 function is lethal, while a knockdown line displayed delayed cotyledon greening and aberrant accumulation of the precursor of the 23S and 4.5S chloroplast rRNAs (Chi et al., 2012). Yeast two-hybrid and pull-down assays indicated that RH22 interacts with PRPL24 in the 50S ribosomal subunit and with a short fragment of the 23S rRNA. RH3 has been characterized in both *A. thaliana* and maize (Asakura et al., 2012; Gu et al., 2014). The *atrh3* null mutant is embryo lethal, while a weak allele (*atrh3-4*) resulted in pale-green seedlings due to defects in splicing of group-II introns and reduced levels of the 50S ribosomal subunit owing to impaired production of 23S and 4.5S rRNAs (Asakura et al., 2012; Gu et al., 2014). A tobacco *RH58/VDL* mutant is defective in plastid differentiation and plant morphogenesis (Wang et al., 2000). The rice homologue of *Arabidopsis* RH50 (OsBIRH1) exhibits RNA helicase activity in vitro, but no direct target of OsBIRH1 has yet been identified (Li et al., 2008).

In *A. thaliana*, RH50 was detected in association with the transcriptionally active chromosome of the plastid (pTAC), together with plastid ribosomal proteins (PRPs), the PEP core enzyme and proteins involved in transcription, translation and RNA metabolism, including RNases and DBRHs (Olinares et al., 2010; Majeran et al., 2012). Helical repeat proteins, such as octatricopeptide (OPRs), pentatricopeptide (PPRs) and tetratricopeptide repeat (TPRs) proteins were also identified in the pTAC complex, in agreement with their primary roles in modulating gene transcription and RNA editing, maturation and stability. Among the PPR proteins identified in the pTAC is GUN1, the product of *GENOMES UNCOUPLED 1* (Koussevitzky et al., 2007). GUN1 integrates information transmitted by several retrograde signaling pathways (Koussevitzky et al., 2007) and physically interacts

120 with several other chloroplast proteins involved in chloroplast protein homeostasis (Tadini et
121 al., 2016). COE1 (Chlorophyll A/B-Binding Overexpression 1)/mTERF4 was recently
122 proposed to form part of a GUN1-mediated retrograde signaling pathway (Sun et al., 2016).
123 Because the *coe1* mutant accumulates high levels of unprocessed RNAs, it was speculated
124 that these unprocessed RNAs might represent a retrograde signal for the down-regulation of
125 nuclear photosynthetic gene expression (Sun et al., 2016).

126 Prompted by the observation that the chloroplast DBRH RH50 and GUN1 have
127 similar expression profiles, we have studied the role of RH50 in plastid gene expression
128 (PGE) and its relationship to GUN1 and retrograde signaling. RH50 promotes the maturation
129 of plastid 23S and 4.5S rRNAs. Moreover, when combined with other mutations affecting
130 PGE, *rh50* in large measure phenocopies *gun1*. These findings imply that GUN1 might also
131 function in the regulation of plastid ribosome biogenesis.
132
133

134

RESULTS

RH50 and GUN1: co-expression and co-localization

We employed a guilt-by-association approach to identify candidate genes involved in plastid protein homeostasis and plastid signaling based on their co-expression with *GUN1*. As part of this effort, mRNA expression data for all predicted plastid-located DBRHs encoded in the *A. thaliana* nuclear genome were compared with the results for the *GUN1* co-expression cluster (as described in Materials and Methods), which itself includes the genes for the plastid ribosomal protein S1 (*PRPS1*), two tetrapyrrole biosynthesis enzymes (the protoporphyrinogen oxidase (*PPOX*) and the D subunit of the magnesium chelatase (*CHLD*), as well as a set of proteins involved in plastid protein homeostasis (Tadini et al., 2016). This allowed us to identify *RH50* as the chloroplast DBRH gene with the highest degree of co-expression with *GUN1*, *PPOX* and *CHLD* (Fig. 1A), followed by *RH58*. Two additional co-expression clusters are formed by *RH17*, *RH22* and *RH26*, and by *RH11* and *RH52*. The predicted chloroplast DHBRs RH3, RH33 and RH41 could not be included in this analysis, because they are not represented on the ATH1 Affymetrix Array.

Not only are *RH50* and *GUN1* co-regulated, their products were previously shown to be located in pTACs, together with several other DBRHs and components of the protein expression machinery (Koussevitzky et al., 2007; Olinares et al., 2010). To confirm the co-localization of RH50 and GUN1 in pTACs, GUN1-RFP and RH50-GFP protein fusions were transiently co-expressed in *A. thaliana* protoplasts (see Materials and Methods). The GFP and RFP signals could be clearly detected as overlapping fluorescence foci within chloroplasts (Fig. 1B), indicating that RH50 and GUN1 are found in the same subcompartment.

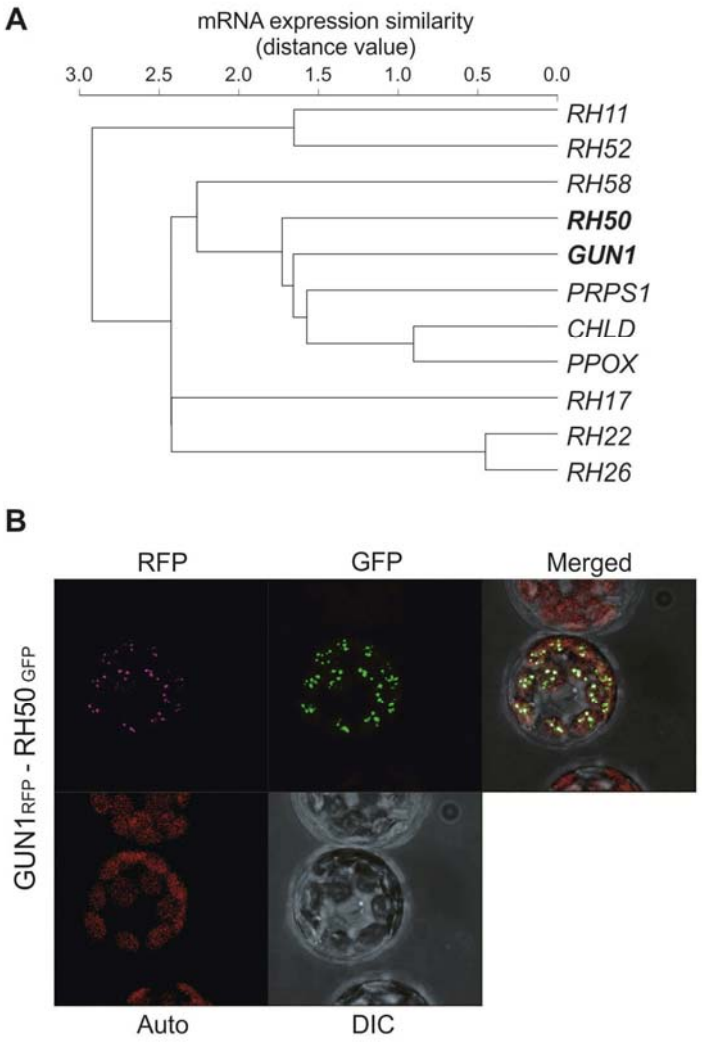

159 ***rh50* is not a *gun* mutant but, like *gun1,* suppresses transcriptional downregulation of**
160 **photosynthesis-associated nuclear genes (PhANGs)**

161 Because *RH50* and *GUN1* are co-regulated at the mRNA level and their products are located
162 in the same chloroplast sub-compartment, we investigated whether, like GUN1 (Tadini et al.,
163 2016), RH50 plays a role in retrograde signaling and plastid protein homeostasis. To this end,
164 two independent loss-of-function alleles of *RH50* (*rh50-1* and *rh50-2*, Fig. 2A and Materials
165 and Methods) were isolated. In *rh50-1* mutant plants, the mutation is caused by a T-DNA
166 insertion, whereas in *rh50-2* a transposon is inserted in the *RH50* gene. Both insertions are
167 located in the second exon and completely prevent expression of the RH50 protein (Fig. 2B).

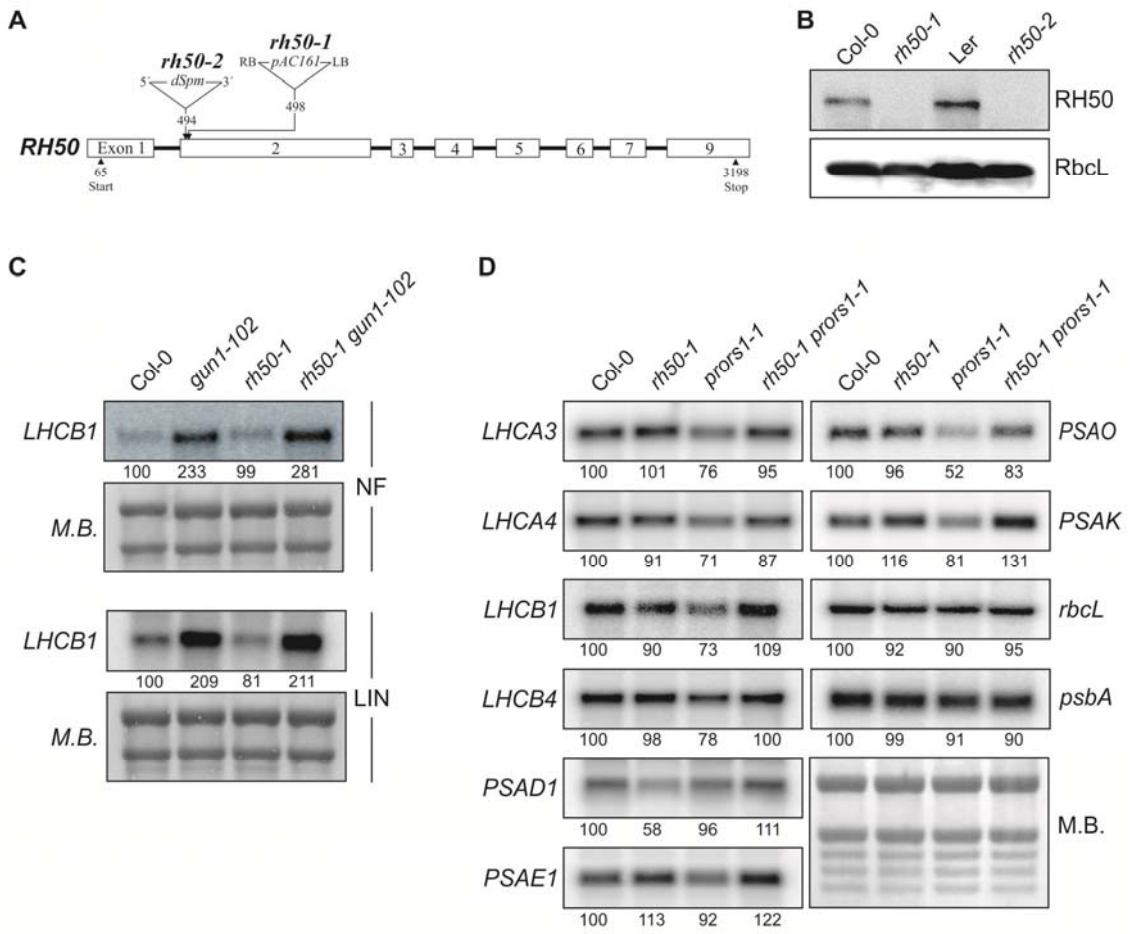

The possible involvement of RH50 in GUN1-mediated retrograde signaling was analyzed by testing whether *rh50-1* seedlings exhibit the *genomes uncoupled* (*gun*) phenotype, i.e., aberrant *LHCB1* expression in the presence of norflurazon (NF) or lincomycin (LIN) (Fig. 2C). However, as in the wild type (WT), *LHCB1* expression was strongly reduced in the *rh50-1* single mutant after treatment with NF or LIN, whereas in *gun1-102* plants, *LHCB1* expression was derepressed. Moreover, in the *rh50-1 gun1-102* double mutant, the *gun* phenotype was unchanged.

To further investigate the involvement of RH50 in PGE-mediated retrograde signaling in adult plants, *rh50-1* was crossed into the *prors1-1* genetic background and the expression of photosynthesis-associated nuclear genes (PhANGs) was assessed (Fig. 2D). The *prors1-1* mutation down-regulates expression of the proline tRNA synthetase1 (PRORS1), thereby

perturbing PGE in adult plants (Pesaresi et al., 2006). Interestingly, the expression of *LHCA3*, *LHCA4*, *LHCB1*, *PSAO* and *PSAK* genes, which is downregulated by about 20-30% in the *prors1-1* mutant, was restored to WT-like levels in *rh50-1 prors1-1* mutant, as in the case of the *gun1-102 prors1-1* double mutant (Tadini et al., 2016).

Thus, like GUN1, RH50 is capable of modulating chloroplast-to-nucleus communication when the PGE machinery is mildly disrupted in mature plants, as in case of *prors1-1*. However, in seedlings and under more severe conditions, such as those induced by treatment with NF or LIN, only GUN1 appears to be critical for plastid signaling.

_rh50_ and _gun1_ mutations display similar patterns of epistasis when combined with mutations affecting PGE

Both synergistic enhancer (*gun1-102 prpl11-1*) and suppressor (*gun1-102 prps1-1*) phenotypes have been observed when the *gun1* mutation was introduced into genetic backgrounds carrying mutations in genes for plastid ribosomal proteins (Tadini et al., 2016). These findings pointed to a functional link between GUN1 and plastid ribosomes. Therefore, to further compare the effects of the *rh50-1* and *gun1-102* mutations on chloroplast function, double mutants combining *rh50-1* or *gun1-102* with several other mutations (*prors1-1*, *prpl11-1*, *prps1-1*, *prps21-1*, *prps17-1* and *prpl24-1*) were generated and characterized (Fig. 3A-F). In contrast to *A. thaliana* plants defective for RH3, 22 or 39, which are characterized by developmental arrest at the embryo stage (Nishimura et al., 2010; Asakura et al., 2012; Chi et al., 2012), both *rh50* mutant alleles behaved like WT with respect to plant size and photosynthetic performance (measured as effective quantum yield of photosystem II (Φ_{II}) after a 15-min exposure to actinic light of 37 μmol photons m^{-2} s^{-1}, see Materials and Methods) under standard growth conditions (Fig. 3A). Interestingly, *rh50-1 gun1-102* plants were markedly smaller than either of the single mutants (Fig. 3A,B), supporting the idea of a

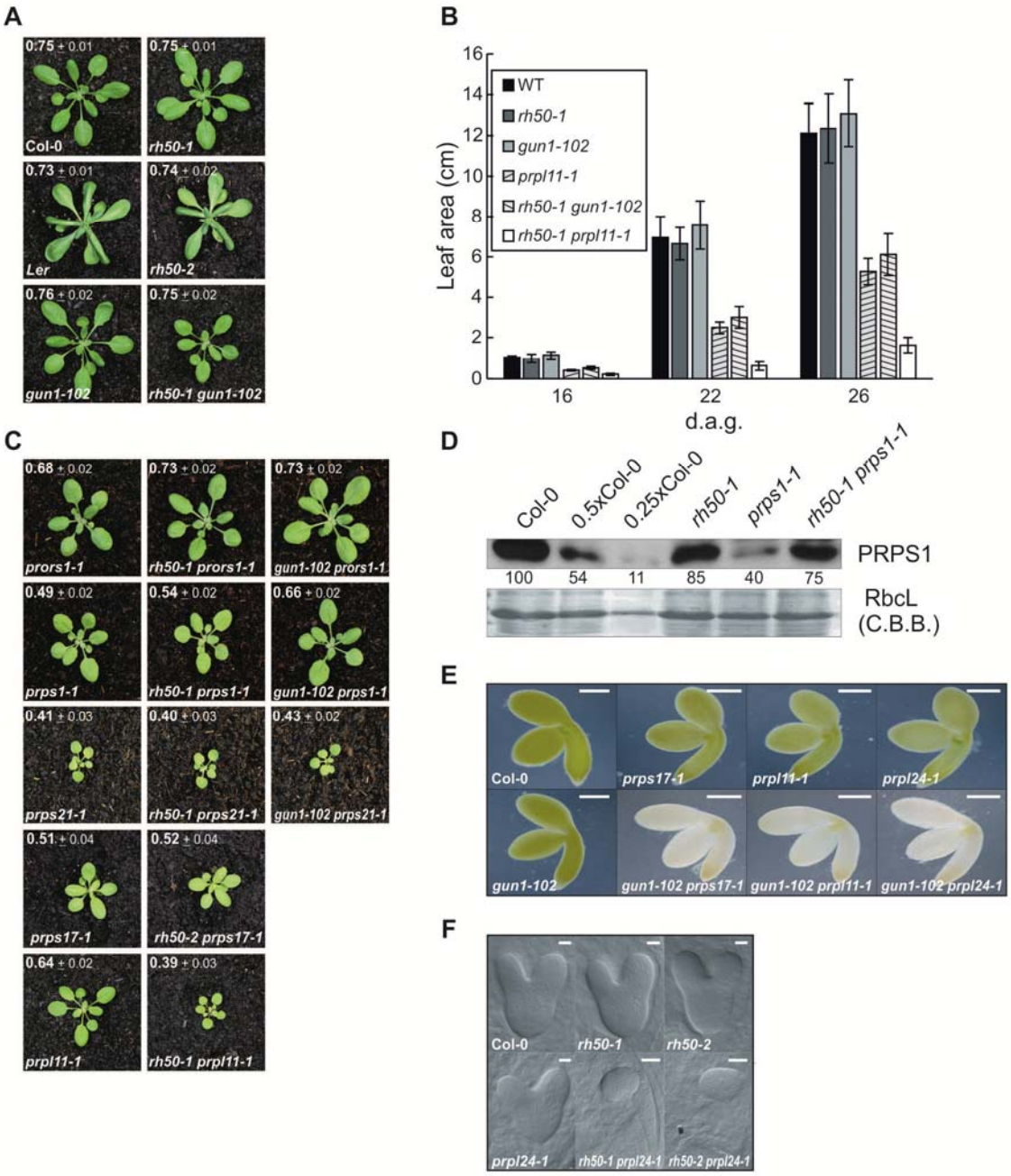

204 functional interaction between *GUN1* and *RH50*, although the photosynthetic performance of
205 adult plants was unaffected.

206 Like *gun1-102*, *rh50-1* restored PhANG expression in the *prors1-1* genetic
207 background (see Fig. 2D). In both cases, this restoration of PhANG expression was
208 associated with increased plant size and improved photosynthetic performance (Φ_{II} of 0.73 ±

209 0.02 for both double mutants versus 0.68 ± 0.02 in *prors1-1*) relative to the *prors1-1* single
210 mutant (Fig. 3C).

211 The *rh50* and *gun1-102* mutant alleles were also combined with mutations affecting
212 proteins of the 30S (*prps1-1, prps17-1* and *prps21-1*) and 50S (*prpl11-1* and *prpl24-1*)
213 subunits of the plastid ribosome. The *rh50-1* mutation partially suppressed the effects of the
214 leaky *prps1-1* mutation on photosynthetic performance, albeit not to the same extent as *gun1-*
215 *102* (*prps1-1*, 0.49 ± 0.02; *rh50-1 prps1-1*, 0.54 ± 0.02; *gun1-102 prps1-1,* 0.66 ± 0.02),
216 whereas *gun1-102 prps1-1* double mutants have larger plant sizes than *prps1-1* plants (Tadini
217 et al., 2016; Fig. 3C). As in the case of the *gun1-102 prps1-1* double mutant (Tadini et al.,
218 2016), the improvement of photosynthetic parameters in the *rh50-1 prps1-1* mutant was
219 associated with increased amounts of PRPS1 protein, from ~40% of the WT level in the leaky
220 *prps1-1* single mutant to ~75% in the *rh50-1 prps1-1* mutant background (Fig. 3D).
221 Complete loss of *GUN1* was previously shown to restore WT-like PRPS1 protein levels in
222 the *prps1-1* background (Tadini et al., 2016). Because the leaky *prps1-1* mutation was due to
223 a T-DNA insertion in the promoter region of the *PRPS1* gene (Romani et al., 2012) that led to
224 a decrease in the accumulation of *PRPS1* transcripts equally in *prps1-1* and *prps1-1 gun1-102*
225 plants, it was previously concluded that GUN1 has a role in protein homeostasis in
226 chloroplasts by contributing to decrease the stability of chloroplast proteins like PRPS1
227 (Tadini et al., 2016). Consequently, also RH50 might have a role, either directly or indirectly,
228 in PRPS1 homeostasis.

229 Of the other two mutations for 30S ribosomal proteins tested, one behaved identically
230 and the other discordantly in *rh50-1* and *gun1-102* backgrounds. While *rh50-1 prps21-1* and
231 *gun1-102 prps21-1* had phenotypes very similar to the *prps21-1* single mutant in terms of
232 plant size and photosynthetic efficiency (Fig. 3C), the phenotype of *rh50-2 prps17-1* differed
233 markedly from that of *gun1-102 prps17-1*. The former was indistinguishable from the

234 *prps17-1* mutant (Romani et al., 2012), showing reduced plant size and reduced
235 photosynthesis compared to the WT (Fig. 3C), whereas *gun1-102 prps17-1* plants were
236 seedling lethal (Fig. 3E). Even more severe effects were observed when *rh50-1* or *gun1-102*
237 was crossed into backgrounds defective for 50S ribosomal proteins (*prpl11-1* and *prpl24-1*).
238 While *gun1-102 prpl11-1* plants were seedling lethal (Tadini et al., 2016, Fig. 3E), the *rh50-1*
239 *prpl11-1* double mutant was viable when grown on soil but strongly affected, relative to the
240 *prpl11-1* single mutant, in terms of growth rate and photosynthesis (Fig. 3B,C). The
241 combination of *rh50-1* with *prpl24-1* resulted in embryo lethality (Fig. 3F), while *gun1-102*
242 *prpl24-1* plants were seedling lethal (Fig. 3E). Growth arrest at the globular stage of embryo
243 development has been reported for several other mutants deficient in plastid ribosomal
244 proteins (like *prps20, prpl1, prpl4, prpl21, prpl27* or *prpl35*) (Romani et al., 2012; Yin et al.,
245 2012).

246 Taken together, these analyses suggest that the loss of *RH50*, like that of *GUN1*,
247 generally tends to potentiate the effects of mutations in genes for plastid ribosomal subunits
248 (such as *prors1*, *prps1*, *prps21*, *prpl11* and *prpl24*). However, loss of *GUN1* provoked more
249 dramatic effects in two cases (*prps1-1* and *prpl11-1*), and only in combination with the
250 *prpl24-1* mutation did the loss of *RH50* lead to a stronger effect than loss of *GUN1*.
251 Moreover, in contrast to *gun1-102*, *rh50-1* did not enhance the *prp17-1* phenotype.

252 These findings imply that many of the epistatic effects of *gun1* in backgrounds
253 containing mutations affecting PGE are not unique. Clearly, both RH50 and GUN1 can
254 mitigate the effects of partial loss of some ribosomal functions at least under the conditions
255 studied here.

256

257 **Functional and physical association of RH50 with the plastid ribosome**

As described above, the strongest epistatic effects of *rh50-1* were observed on mutations in genes for subunits of the large plastid ribosomal subunit (see Fig. 3). To determine whether ribosomes are structurally impaired in the *rh50-1* mutant, we analyzed mutant and WT responses to the antibiotics chloramphenicol, lincomycin and erythromycin, which are known to target the large subunit of the plastid ribosome and prevent elongation of the nascent polypeptide chain, either by binding to the peptidyltransferase center (chloramphenicol and lincomycin) or by blocking the exit tunnel (erythromycin) (Sohmen et al., 2009). The *rh50-1* mutant showed a WT-like phenotype when treated with lincomycin and chloramphenicol, but was clearly more sensitive to erythromycin, as mutant seedlings were smaller and paler than, and exhibited reduced photosynthetic efficiency relative to, WT seedlings (Fig. 4A).

Defects in plastid translational capacity are often associated with impaired acclimation to cold, as reported previously in mutants defective for *PRPL33*, *PRPS5* or *RDB1* (Rogalski et al., 2008; Wang et al., 2016; Zhang et al., 2016). Therefore, we quantified cold acclimation in both *rh50-1* mutants and WT plants. Under standard growth conditions, 7-day-old *rh50-1* mutant seedlings showed a reduction in maximum quantum yield of photosystem II compared to the WT (F_V/F_M 0.67 ± 0.01 *versus* 0.77 ± 0.01, respectively) (Fig. 4B), a phenotype which is lost in adult plants (see Fig. 3A). Intriguingly, *rh50-1* mutants are less tolerant than WT to cold stress. In *rh50-1* seedlings, germinated and grown on MS medium supplemented with 1% sucrose for 6 weeks at 4°C and then transferred to 22°C, growth rate, chlorophyll accumulation and F_V/F_M (*rh50-1*: 0.27 ± 0.07; WT: 0.72 ± 0.02) were all adversely affected (Fig. 4B). In the absence of sucrose, this phenotype was exacerbated, as *rh50-1* mutants completely failed to accumulate chlorophyll, and died as seedlings (Supplemental Fig. S1). Furthermore, reducing the light intensity to lessen oxidative stress (see Material and Methods) failed to rescue cold-treated *rh50-1* seedlings (Supplemental Fig. S1).

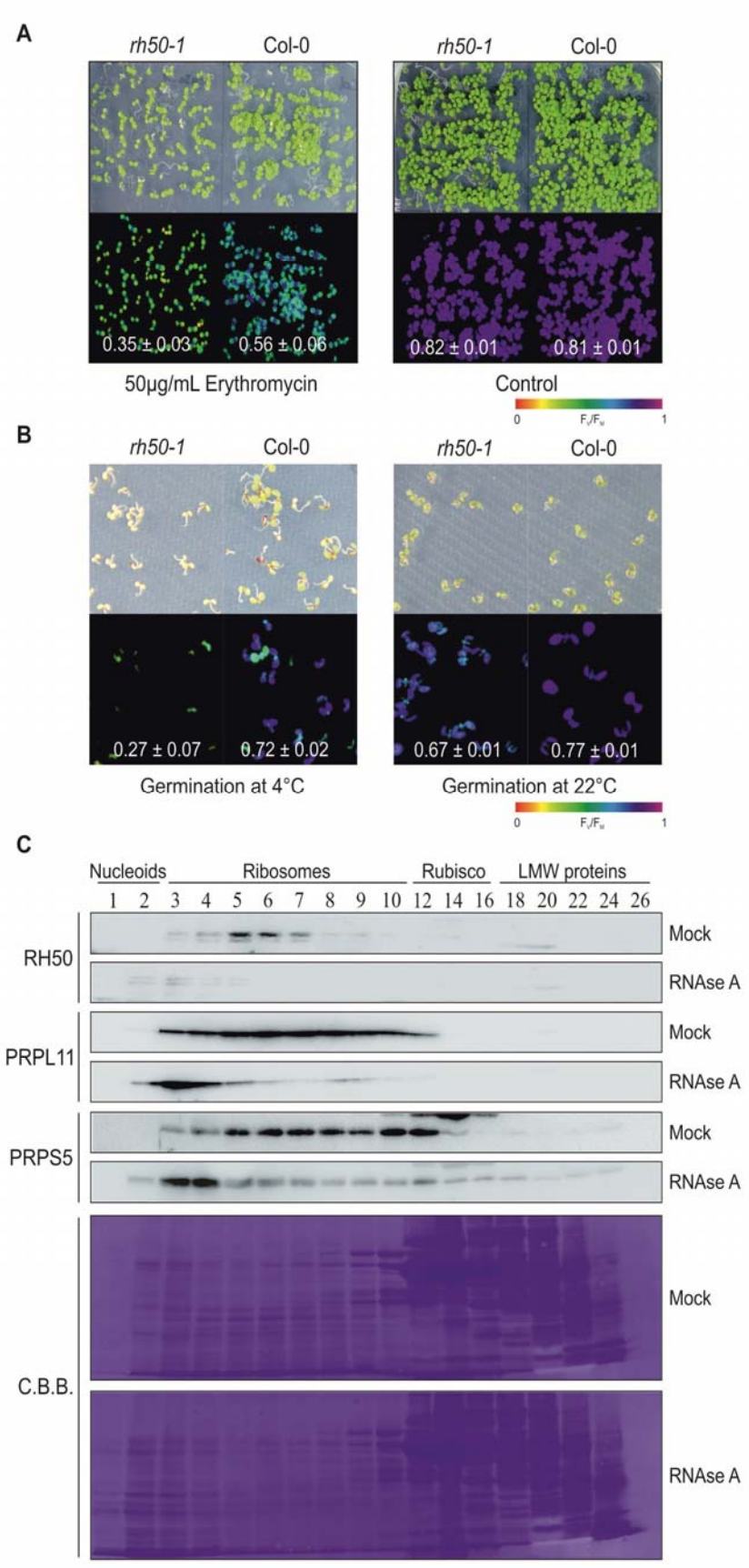

282 To investigate whether RH50 physically interacts with plastid ribosomal proteins,

283 yeast two-hybrid (Y2H) assays were performed. In these experiments, RH50 was employed
284 as bait (Bd vector) and tested for binding to GUN1, RPL11, RPL24, RPS1, RPS17 and
285 RPS21 as prey proteins (Ad vectors). Apart from the previously described $GUN1^{BD}$-$CHLD^{AD}$
286 interaction (Tadini et al., 2016), used as positive control, no further binding interactions were
287 detected (see Supplemental Fig. S2).

288 To test whether RH50 associates with intact ribosomes *in vivo*, size-exclusion
289 chromatography of soluble chloroplast stroma extracts was conducted. As previously
290 described (Olinares et al. 2010), RH50 was identified in megadalton complexes (with a main
291 peak in fractions 5-7), co-migrating with ribosomal particles, as demonstrated by
292 immunodetection using RH50-, PRPL11-, and PRPS5-specific antibodies (Fig. 4C).
293 Moreover, when extracts were treated with RNase, RH50 was no longer detectable in
294 fractions 5-7, indicating that the protein associates with RNA-containing and RNase-sensitive
295 particles. A similar trend was observed for proteins of the large and small ribosomal subunit,
296 pointing to the association of RH50 with immature ribosomes, which are more accessible for
297 RNases than the mature forms found in fractions 3 and 4.

298 Thus, loss of RH50 increases sensitivity to erythromycin – an inhibitor that binds to
299 the large ribosomal subunit – and to cold stress. In fact, several DBRHs have been reported to
300 be involved in adaptation to cold stress. RH7 plays a role in pre-18S rRNA processing and
301 small ribosome subunit biogenesis, and promotes plant development at low temperatures
302 (Huang et al., 2016; Liu et al., 2016). The cytosolic RH5, RH9 and RH25 helicases are
303 involved in the response to both salt and cold stresses (Kant et al., 2007; Kim et al., 2008),
304 while the plastid-localized RH3, which is required for intron splicing, mediates salt- and
305 cold-stress responses (Larkin et al., 2003; Gu et al., 2014). Moreover, RH50 associates with
306 RNA-containing megadalton complexes that are RNase sensitive and contain ribosomal
307 proteins, suggesting that RH50 interacts with immature chloroplast ribosomes, possibly as a

ribosomal biogenesis factor. These observations are compatible with the co-migration of the well characterized, plastid-localized RH22 with ribosomes (Chi et al., 2012), and with the presence of RH50 in pTACs, which also contain ribosomes (Majeran et al., 2012).

Lack of RH50 affects translational capacity in chloroplasts

Because the results described above point to a function of RH50 in chloroplast ribosomal biogenesis, the translational capacity of *rh50* chloroplasts was also investigated. To this end, WT and *rh50-1* seedlings were exposed to cold treatment and non-stressed conditions as described in Fig. 4B and polysome-loading experiments were performed (Fig. 5A, Supplemental Fig. S3). We chose to examine *psaA* mRNA, which is efficiently loaded onto polysomes and hence migrates deep into the sucrose gradient (Amann et al., 2004; Meurer et al., 2017). Under non-stressed conditions, loading of *psaA* mRNA onto *rh50* polysomes was indistinguishable from the one onto WT polysomes with the peak fractions 9-11 (Supplemental Fig. S3). After cold treatment *psaA* transcripts were clearly shifted towards the low-molecular-weight fractions in WT and *rh50-1* plants, and the effect was more drastic in *rh50-1* (peak fractions 5-8) than in the WT (peak fractions 7-9) (Fig. 5A).

Rates of protein synthesis in chloroplasts were then evaluated by *in vivo* labeling in extracts of WT, *rh50-1*, *prpl11-1* and *rh50-1 prpl11-1* plants, since the double mutant displayed a synergistic growth and photosynthesis phenotype. To this end, the rate of incorporation of ^{35}[S]methionine into plastid proteins was monitored at the 6-leaf rosette stage after 5, 10 and 15 min of light exposure (Fig. 5B). Cytosolic synthesis of nucleus-encoded proteins was chemically inhibited with cycloheximide (see Materials and Methods). Total proteins were then extracted, fractionated by SDS-PAGE, and the radioactivity incorporated into D1 and D2 proteins was determined. The overall rate of synthesis observed was slightly reduced in the *rh50-1* and *prpl11-1* single mutants with respect to WT plants

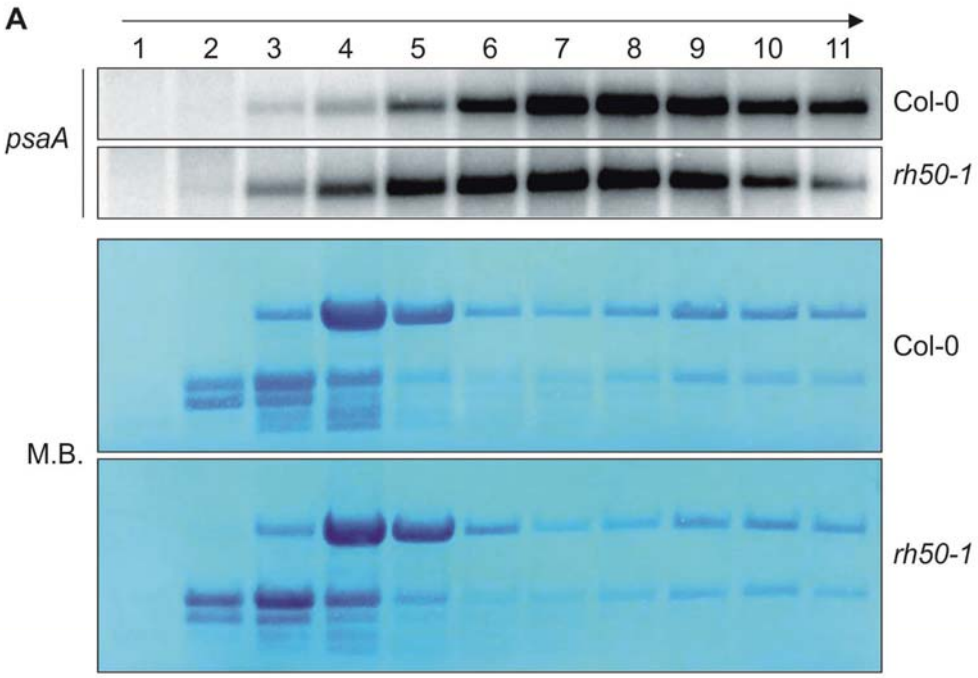

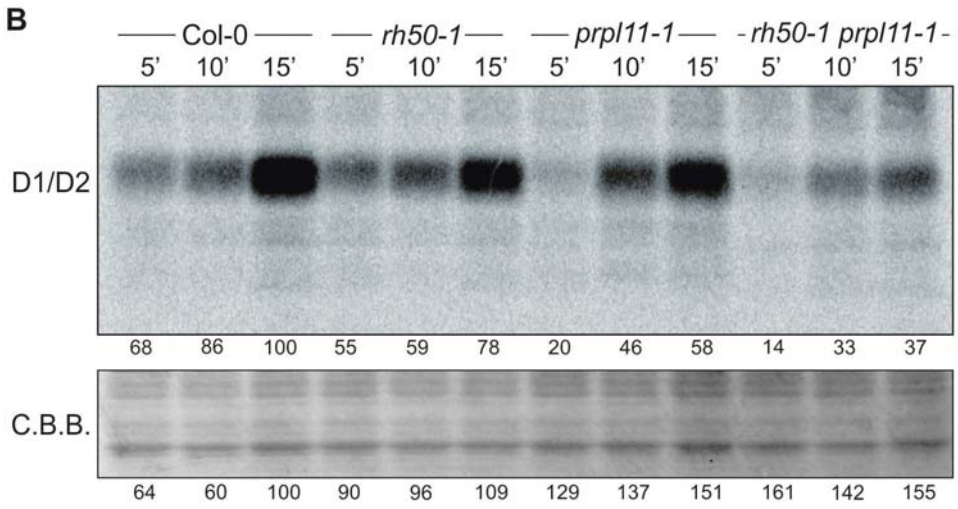

and, as expected, the double mutant was markedly less active than either parental genotype at all three time points, reaching only 37% of the WT incorporation level after 15 min (Fig. 5B).

Taken together, these results confirm that lack of RH50 impairs translation in chloroplasts and exacerbates the impact of the relative loss of the plastid ribosomal protein L11.

339 **RH50 is involved in plastid rRNA metabolism**

340 To investigate the role of RH50 in chloroplast RNA metabolism, RNA-seq analysis was
341 performed on total RNA extracted from 3-week-old WT and *rh50-1* plants (Supplemental
342 Table S1 and Supplemental Fig. S4). Expression of nuclear genes was largely unaffected in
343 *rh50-1* plants (Supplemental Table S1). However, inspection of chloroplast gene expression
344 revealed a marked increase in levels of transcripts derived from the *rrn23S-rrn4.5S* intergenic
345 region in the mutant, as well as less pronounced changes in 16S rRNA and mRNAs for Rpl2
346 and Rpl23 (Supplemental Fig. S3, Fig. 6A).

347 To corroborate the RNA-seq data, accumulation of plastid rRNAs in WT (Col-0) and
348 *rh50-1* plants was investigated by RNA blot analyses (Fig. 6B,C). Plants carrying the *gun1-*
349 *102* or *gun1 rh50-1* mutations were included, since *gun1-102* and *rh50-1* interact with
350 ribosomal mutations in similar ways based on the growth phenotype of resulting double
351 mutants (see Fig. 3). In the WT, the polycistronic plastid rRNA operon (*rrn16–trnI-trnA-*
352 *rrn23S-rrn4.5S-rrn5S*) is transcribed as a single RNA molecule and further processed by
353 various nucleases, generating as intermediate products a 16S precursor, a bicistronic 23S-
354 4.5S precursor and a 5S precursor (Shajani et al., 2011). The 23S-4.5S precursor (3.2 kb)
355 undergoes endonucleolytic cleavage to produce 4.5S (*rrn4.5S*) and 23S RNA (*rrn23S*)
356 fragments (2.9 kb). The 23S precursor is then further processed and eventually gives rise to
357 mature transcripts of 1.3 kb, 1.1 kb and 0.5 kb in the chloroplast ribosome (Bollenbach et al.,
358 2005). These processing steps and the probes used for RNA gel-blot analyses are summarized
359 in Fig. 6B. The data showed that *rrn16S* and *rrn4.5S* rRNA transcripts (detected with probes
360 a and e, respectively; Fig. 6B) accumulate to the same levels in the WT and all mutant
361 backgrounds analyzed (Fig. 6C). However, RNA blots hybridized with probes specific for
362 *rrn23S* (b) and *rrn4.5S* (d) revealed defects in the processing of *rrn23S* and *rrn4.5S*
363 transcripts in the absence of RH50. In both *rh50-1* and *rh50-1 gun1-102* mutants, levels of

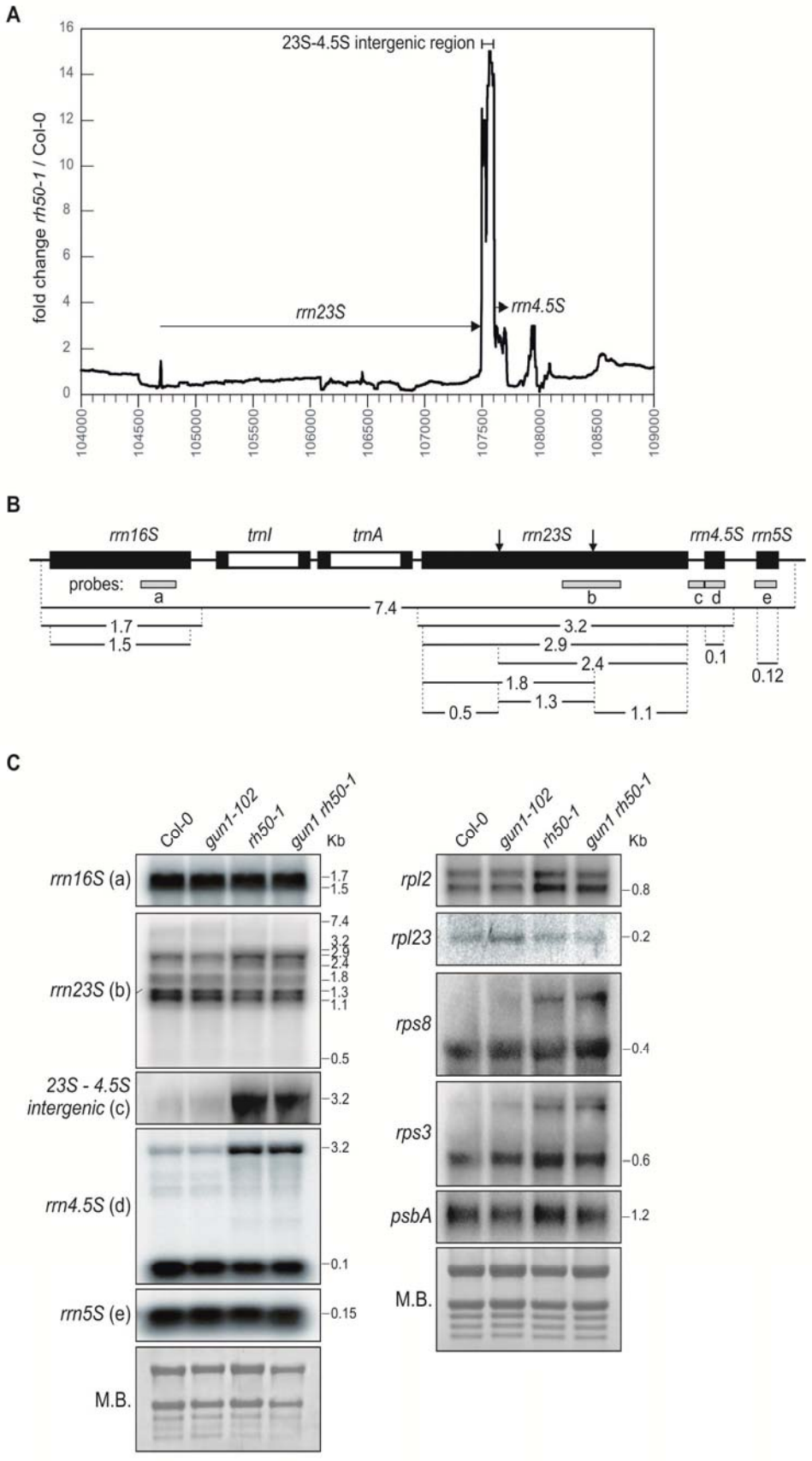

364 mature *rrn23S* and *rrn4.5S* transcripts appeared slightly reduced, while unprocessed

transcripts were enriched relative to WT and *gun1-102*. RNA blots probed with the 23S-4.5S intergenic region probe (c) showed only a barely detectable signal in WT and *gun1-102*, while transcripts of this region accumulated ~7-fold in *rh50-1* and *gun1-102 rh50-1* mutants (Fig. 6C). These findings strongly suggest that RH50 is required for correct processing of RNA sequences derived from the 23S-4.5S intergenic region. Since the *gun1-102 rh50-1* double mutant behaves like *rh50-1*, GUN1 evidently plays no role in this pathway.

Furthermore, the level of the mature *rpl2* transcript was increased in *rh50-1* and *gun1-102 rh50-1* mutants, confirming the trend found by the RNA-seq analysis, whereas no differences in transcript accumulation were observed for *rpl23*. In the case of *rps8* and *rps3*, processing defects were observed, as increased amounts of the precursor forms were detected in *rh50-1* and *gun1-102 rh50-1* mutants (Fig. 6C) similar to the effects seen for the rRNAs. Since no defect in the steady-state levels of the mature mRNAs was noticed, this is probably a secondary effect of the overall perturbation of the translation machinery (Fristedt et al., 2014). No processing defect was observed for *psbA*.

Taken together, these results imply that maturation of *rrn23S* and *rrn4.5* RNAs is affected in the *rh50-1* mutant, providing a plausible explanation for the impairment of ribosome biogenesis and functionality.

RH50 associates with the 23S-4.5S intergenic region

Because RH50 is required for maturation of the *rrn23S* and *rrn4.5S* RNAs and the processing intermediate *rrn23S-rrn4.5S* strongly accumulates in *rh50-1* (see above), we asked whether RH50 interacts directly with the *rrn23S-rrn4.5S* precursor. To this end, RNA-immunoprecipitation experiments were performed with WT stroma extracts, employing an RH50-specific antibody and the pre-immune serum as a control. The specificity of the antibody was checked by a western blot analysis, which confirmed that it was able to

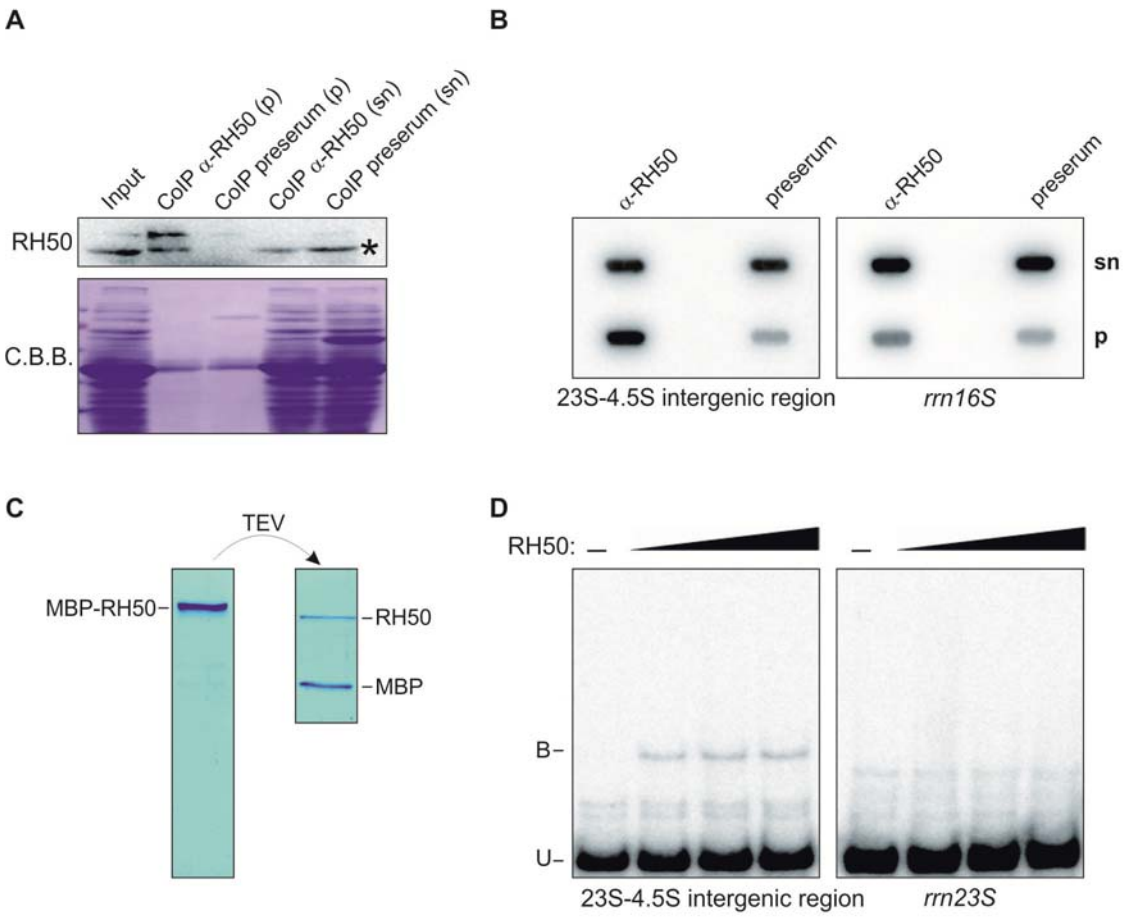

precipitate the RH50 protein (Fig. 7A). Slot-blot analysis of co-precipitated RNAs revealed that the *rrn23S-rrn4.5S* intergenic region was highly enriched in the pellet fraction of the IP performed with anti-RH50 antibodies (ratio pellet/supernatant: 0.80), while a control RNA of similar abundance, *rrn16S*, was much less enriched (ratio pellet/supernatant: 0.18) (Fig. 7B). To verify that RH50 binds directly to the *rrn23S-rrn4.5S* RNA species, an electrophoretic mobility shift assay (EMSA) was performed utilizing affinity-purified recombinant RH50 protein, a radiolabelled probe for the *rrn23S-rrn4.5S* intergenic region and, as a control, the upstream region adjacent to the *rrn23S* RNA (Fig. 7C,D). A shift in electrophoretic mobility was only observed for the *rrn23S-rrn4.5S* RNA (Fig. 7D), implying that RH50 – like RH22 (which binds to the 5' region of the 23S rRNA; Chi et al., 2012) and RH39 (that binds to a

23S rRNA segment close to the hidden break; Nishimura et al., 2010) – recognizes a specific rRNA target.

Taken together, our results thus indicate that RH50 promotes the maturation of 23S and 4.5S rRNAs by binding to the *rrn23S-rrn4.5S* intergenic region in the precursor rRNA. We speculate that RH50, as an RNA helicase, unwinds double-stranded segments in this region to facilitate cleavage by a sequence-specific endonuclease.

406

DISCUSSION

RH50 promotes biogenesis of the plastid ribosome by facilitating the processing of *rrn23S-rrn4.5S* rRNA

Ribosome biogenesis is a complex, multistep process that requires transcription of the ribosomal gene cluster, rRNA processing and ribosome assembly (Kaczanowska and Rydén-Aulin, 2007). Several factors involved in plastid ribosome biogenesis have been described. Among these, RHON1 was shown to bind the intercistronic region of the *rrn23S-rrn4.5S* RNA precursor and to specify the sequence cleaved by the Arabidopsis endonuclease RNaseE (Stoppel et al., 2012); SUPPRESSOR OF THYLAKOID FORMATION1 (SOT1), a plastid-localized pentatricopeptide repeat protein, is also required for correct processing of 23S-4.5S rRNA precursor (Wu et al., 2016) while RAP, an octotricopeptide repeat protein, binds to the 5' region of the 16S rRNA precursor and promotes its maturation (Kleinknecht et al., 2014). Furthermore, the chloroplast DBRH RH39 plays an essential role in introducing the hidden break into the 23S rRNA, acting together with an as-yet unidentified endonuclease (Nishimura et al., 2010). A second plastid-localized DBRH, RH22, stimulates assembly of the 50S ribosomal subunit by participating in the processing of 23S rRNA and, at the same time, binding to the ribosomal protein RPL24 (Chi et al., 2012).

In this study, we present multiple lines of evidence for the involvement of a third DBRH, RH50, in chloroplast rRNA metabolism. In *rh50-1* plants, absence of RH50 renders protein synthesis in the chloroplast abnormally sensitive to erythromycin and low temperatures (see Fig. 4), while polysome loading is perturbed in cold-acclimated plants and translation efficiency is reduced under standard growth conditions (see Fig. 5). Furthermore, genetic analyses reveal interactions between *rh50-1* and mutations in genes for proteins of the 50S ribosomal subunit (see Fig. 3), and in WT plants RH50 associates with ribosomal

particles (see Fig. 4). Finally, we show that maturation of the *rrn23S-rrn4.5S* processing intermediate is impaired in *rh50-1* plants (see Fig. 6), and that affinity-purified RH50 binds specifically to the *rrn23S-rrn4.5S* intergenic region, as demonstrated by immunoprecipitation and EMSA experiments (see Fig. 7).

A role for RH50 in rRNA processing can also account for the cold sensitivity of *rh50-1* plants (see Fig. 4B). Several previous studies have suggested that RNA helicases play a pivotal role in plant stress responses (Liu et al., 2002; Owttrim, 2006; Vashisht and Tuteja, 2006; Kant et al., 2007; Nawaz and Kang, 2017). Since these enzymes mediate localized unwinding of RNAs, they might well become critical at low temperatures, which are expected to stabilize RNA secondary structure (Herschlag, 1995; Jones and Inouye, 1996; Lorsch, 2002). In fact, the cytosolic RH7, which is involved in pre-18S rRNA processing and biogenesis of the small (40S) ribosomal subunit, is essential for plant development at low temperatures (Huang et al., 2016; Liu et al., 2016). Moreover, the helicases RH5, RH9 and RH25 contribute to the response to salt and cold stresses (Kant et al., 2007; Kim et al., 2008), and the plastid-located RH3, which is required for intron splicing, mediates salt- and cold-stress responses (Gu et al., 2014).

The functional relationship between RH50, GUN1, and plastid signaling

GUN1 interacts genetically with *PRPL11* and *PRPS1*, and its product binds to the chloroplast ribosomal protein PRPS1 (Tadini et al., 2016). In this study, these interaction studies were extended by comparing the epistatic effects of *rh50-1* and *gun1-102* on additional mutations affecting chloroplast ribosomal proteins. Clearly, loss of *RH50* and *GUN1* modulates the effects of selected ribosomal mutations in similar ways. Generally speaking, combinations of *rh50-1* or *gun1-102* with *prps17-1*, *prps21*, *prpl11* or *prpl24* tend to potentiate the phenotypes of the respective single mutants, with *gun1-102* having the more dramatic effect

than *rh50-1* when combined with *prps17-1* or *prpl11-1*, and *rh50-1* inducing a stronger effect than loss of *GUN1* in the case of the *prpl24-1* mutation. With respect to the *prps1-1* and *prors1-1* mutations, both *rh50-1* and *gun1-102* act as suppressor mutations (Tadini et al., 2016 and this study). These findings concerning loss of RH50 are consistent with previous observations, which implied that several RNA helicases, specifically RH3, RH39 and RH22, interact with ribosomal proteins (Nishimura et al., 2010; Asakura et al., 2012; Chi et al., 2012).

In addition to the similar behavior of double mutants that lack either RH50 or GUN1, there are additional similarities between the two genes and their mutants. In fact, *RH50* is co-regulated with *GUN1* (see Fig. 1A), RH50 and GUN1 are located in the same subcompartment (see Fig. 1B), and *rh50-1* – like *gun1-102* (Tadini et al., 2016) – suppresses the down-regulation of PhANG expression seen in the *prors1-1* mutant (see Fig. 2D). However, unlike *gun1-102*, *rh50-1* itself does not induce the classical *gun* phenotype observed in seedlings exposed to NF or LIN (see Fig. 2C). So, what can we learn from these results with respect to the function of GUN1? Based on the similarities of GUN1 and RH50 outlined above and our finding that RH50 has a role in rRNA metabolism and appears to interact with immature plastid ribosomes (Figs. 4-7), it is tempting to speculate that also GUN1 has a function that is related to ribosome biogenesis or its functionality. But clearly, the mechanism by which GUN1 exerts this function differs from that of RH50, since GUN1 appears to bind proteins rather than RNAs (Tadini et al., 2016).

Conclusion

RH50 is a plastid rRNA maturation factor that possibly interacts with immature ribosomes and consequently its absence affects the functionality of ribosomes. The similarities between RH50 and GUN1, in particular with respect to the behavior of their mutants, allows us to

speculate that GUN1 might also have a function in plastid ribosome biogenesis and functionality. Future studies aimed to clarify the function of GUN1 and its interplay with ribosome biogenesis might take advantage of the observed double mutant phenotypes observed in this study, for instance by designing genetic suppressor screens to identify mutations that behave like *gun1* in suitable double mutants.

MATERIALS AND METHODS

Plant material, propagation and growth measurements

The *Arabidopsis thaliana* T-DNA insertion mutant line *rh50-1* (GABI_629A10, genetic background Col-0) was obtained from the GABI-KAT collection (Rosso et al., 2003) and the transposon line *rh50-2* (GT_5_111858, genetic background L*er*) from the GT collection (http://gt.jbei.org/arabidopsis.html). The regions flanking the insertions were PCR-amplified and sequenced (primer sequences in Supplemental Table S2), and both the T-DNA and the transposon were found to lie in exon 2 (at positions 433 and 429 relative to the start codon, respectively). In addition, the following previously described mutant lines were used in this work: *gun1-102* and *prps21-1* (Tadini et al., 2016)*, prors1-1* (Pesaresi et al., 2006)*, prpl11-1* (Pesaresi et al., 2001), *prps1-1*, *prps17-1* and *prpl24-1* (Romani et al., 2012b).

A. thaliana plants were grown on soil in a climate chamber as described (Pesaresi et al., 2009). For treatment with norflurazon or antibiotics, surface-sterilized mutant and WT seeds were plated on Murashige and Skoog (MS) medium (PhytoTechnology Laboratories, LLC™, USA) containing 1% (w/v) sucrose and 0.8% (w/v) agar supplemented with either 5 μM norflurazon (Sandoz Pharmaceuticals, Vienna, Austria), 220 μg ml^{-1} lincomycin (Sigma, St Louis, MO, USA), 50 μg ml^{-1} erythromycin (Sigma-Aldrich, Munich, Germany) or 40 μg ml^{-1} chloramphenicol (Sigma-Aldrich). For the cold stress treatments, surface-sterilized mutant and WT seeds were plated on MS medium containing 1% (w/v) sucrose. The seeds were allowed to germinate in a climate chamber at 4°C under long-day conditions (16 h light/8 h dark) and either standard levels of light or low light (100 or 30 μmol photons s^{-1} m^{-1}) for 6 weeks and then transferred at 22°C under same long-day conditions.

For growth measurements, leaf area was determined with the ImageJ software (http://imagej.nih.gov/ij/index.html).

515

516 **Transient co-expression of *GUN1* and *RH50* cDNAs in *A. thaliana* leaf protoplasts**

517 *GUN1* and *RH50* cDNA were cloned without their stop codons into the Gateway entry vector
518 pDONR207 (Invitrogen; Carlsbad, CA) as described (Tadini et al., 2016). The entry vector
519 was then recombined with pK7RWG2 and pB7FWG2 (Vinti et al., 2000) to generate 35S
520 promoter-driven C-terminal GUN1-RFP and RH50-GFP fusions.

521 Two-week-old WT *Arabidopsis* seedlings were cut into small pieces and incubated for
522 16 h at 24°C in the dark in a protoplasting solution (10 mM MES, 20 mM $CaCl_2$, 0.5 M
523 mannitol (pH 5.8) containing 0.1 g mL^{-1} macerozyme and 0.1 g mL^{-1} cellulase [both from
524 Duchefa, Haarlem, The Netherlands]). Protoplasts were then isolated as described previously
525 (Dovzhenko et al., 2003) and transfected with the GUN1-RFP and RH50-GFP constructs by
526 the calcium-PEG method. Protoplasts were incubated for 24 h, and then assessed for fusion
527 gene expression with a confocal microscope (Leica TCS SP5 CLSM).

528

529 **Chlorophyll *a* fluorescence measurements**

530 Five plants of each genotype were analyzed, and average values and standard deviations were
531 calculated. *In vivo* chlorophyll *a* fluorescence of single leaves was measured using the Dual-
532 PAM 100 (Walz, Germany). Pulses (0.5 s) of saturating light (5,000 μmol photons m^{-2} s^{-1})
533 were used to determine the maximum fluorescence (F_M) and the ratio $(F_M - F_0)/F_M = F_V/F_M$,
534 where F_0 is the minimum fluorescence. A 15-min exposure to actinic light (37 μmol photons
535 m^{-2} s^{-1}) was used to drive electron transport before measuring Φ_{II} (Armbruster et al., 2010).
536 *In vivo* Chl a fluorescence of whole plants was recorded using an imaging Chl fluorometer
537 (Imaging PAM; Walz, Germany). Dark-adapted plants were exposed to a pulsed, blue
538 measuring beam (1 Hz, intensity 4; F0) and a saturating light flash (intensity 4) to obtain
539 F_V/F_M.

Co-expression analysis

To identify genes represented on the ATH1 Affymetrix microarray (22K) chip that show a significant degree of co-expression with *GUN1*, an expression correlation analysis was performed with the CoExSearch tool implemented in ATTED-II (http://atted.jp/; Obayashi et al., 2007; Obayashi et al., 2009). Hierarchical clustering was done with the single-linkage method using the HCluster tool in ATTED-II.

Transcriptome sequencing and analysis

Total RNA was extracted from 3-week-old wild-type and *rh50-1* plants, using standard TRizol extraction. RNA was tested for quality by spectrophotometry, agarose gel electrophoresis and PCR. RNA-Seq library preparation and long non-coding RNA sequencing (lncRNAs) were both performed at Novogene Biotech (Beijing, China) using standard Illumina protocols. The RNA-Seq libraries were sequenced using the paired-end mode on an Illumina HiSeq 2500 system. At least three biological replicates were used for each analysis.

The quality of the raw data was verified with FASTQC (http://www.bioinformatics.babraham.ac.uk/projects/fastqc/). Sequences were filtered and trimmed using Trimmomatic (http://www.usadellab.org/cms/?page=trimmomatic) (Bolger et al., 2014). Reads were mapped to the Arabidopsis reference genome (TAIR10) using HISAT with default parameter settings (https://ccb.jhu.edu/software/hisat/index.shtml). Transcript assembly and FPKM (RPKM) values were calculated using htseq-count (http://www-huber.embl.de/HTSeq/doc/count.html, version of 2016). Deregulated genes were identified with DESeq2 (https://bioconductor.org/packages/release/bioc/html/DESeq2.html) (Love et

565 al., 2014). All of these analyses were performed using a local Galaxy server
566 (http://galaxyproject.org) (Giardine et al., 2005).

567 To obtain a more detailed view of the chloroplast genome, the reads from WT and
568 *rh50-1* were mapped to the chloroplast genome of *Arabidopsis* using the Qiagen CLC
569 Genomics Workbench v.8.5.1 (hereafter CLC). Before assembly, the reads were trimmed
570 using CLC with default settings. The trimmed sequences were then mapped to the chloroplast
571 genome of *Arabidopsis thaliana* (NC_000932.1). Fold changes were calculated and
572 visualized with Excel.

573

574 **Nucleic acid analysis**

575 *A. thaliana* genomic DNA was isolated as described (Ihnatowicz et al., 2004) and RNA was
576 purified from frozen leaf tissue as described before (Armbruster et al., 2010). RNA gel-blot
577 analyses were performed under stringent conditions (Green and Sambrook, 2012) using 5-µg
578 samples of total RNA. Primers used to amplify the probes are listed in Supplemental Table 2.
579 cDNA fragments were used, except in the case of the 23S-4.5S rRNA intergenic region, for
580 which 5'-end ^{32}P-labeled ssDNA was employed. Signals were quantified with the ImageJ
581 software (http://imagej.nih.gov/ij/index.html).

582

583 **Immunoblot analyses**

584 Immunoblot analyses were carried out as described (Ihnatowicz et al., 2004), using antibodies
585 directed against GFP (Life Technologies, Carlsbad, USA), RbcL (Agrisera, Vännäs,
586 Sweden), PRPS1 (Agrisera), PRPS5 (Agrisera), PRPL11 (Meurer et al., 2017), or RH50
587 (GenScript). The RH50 antibody was raised against the peptide CDNERGLRGGSHSKG.
588 Signals were quantified with ImageJ software (http://imagej.nih.gov/ij/index.html).

589

590 **Yeast two-hybrid and polysome analyses**

591 For yeast two-hybrid assays, the coding sequences of the mature proteins (without the
592 chloroplast transit peptides cTP) of interest (see Supplemental Table S2 for primer
593 sequences) were cloned into pGBKT7 (RH50) and pGADT7 (GUN1, PRPS21, PRPS17,
594 PRPL11 and PRPL24) vectors (Clontech, Otsu, Japan), or *vice versa*. Interactions in yeast
595 were then analyzed as described before (DalCorso et al., 2008).

596 Polysome loading experiments were conducted as described (Barkan, 1993).

597

598 ***In vivo* translation assay**

599 The *in vivo* translation assay was performed essentially as described previously (Tadini et al.,
600 2016). Twelve leaf discs (4 cm diam.) were incubated in a buffer containing 20 μg ml^{-1}
601 cycloheximide, 1 mM K_2HPO_4/KH_2PO_4 (pH 6.3), and 0.1% (w/v) Tween-20 to block
602 cytosolic translation. Then [^{35}S]methionine was added to the buffer (0.1 mCi ml^{-1}) and the
603 material was vacuum-infiltrated. Leaves were exposed to light (20 μmol photons m^{-2} s^{-1}) and
604 four leaf discs were collected at each time point (5, 15 and 30 min). Total proteins were
605 extracted as described (Martinez-Garcia et al., 1999) and loaded on glycine SDS-PA (12%
606 PAA) gels. Signals were detected and quantified using a PhosphoImager (GE Healthcare Life
607 Sciences, www3.gehealthcare.com) and the program Image Quant (GE Healthcare Life
608 Sciences).

609

610 **Co-immunoprecipitation and slot-blot analysis**

611 Chloroplasts from 3-week-old WT plants were isolated as described previously (Stoppel et
612 al., 2012). Lysis was achieved by passing the chloroplast-containing solution (30 mM HEPES
613 pH 8.0, 10 mM Mg acetate, 60 mM K acetate, freshly added Protease Inhibitor Cocktail
614 [Roche, Risch-Rotkreuz, Switzerland]) through a 0.45-mm needle 25 times. Lysates were

615 cleared by centrifugation at 45,000 g for 30 min at 4°C. Samples (each equivalent to 1 mg of
616 stroma) were diluted with the same volume of Co-IP buffer (20 mM Tris pH 7.5, 150 mM
617 NaCl, 1 mM EDTA, 0.5% Nonidet P40, Protease Inhibitor Cocktail [Roche]) and incubated
618 either with RH50-specific antibodies (30 µl) or with the corresponding pre-serum (2 µl) for 1
619 h at 4°C, and then with 50 µl of SiMAG-Protein G beads (Chemicell, Berlin, Germany) for a
620 further hour. Washing, RNA extraction and slot-blot analysis were performed as described
621 previously (Meurer et al., 2017)
622
623 **Production of recombinant RH50 and its use in EMSA**
624 The *RH50* sequence encoding the mature RH50 protein was cloned into the BamHI-SalI sites
625 of the pMAL-Tev vector. The coding sequence for Strep-Tag (WSHPQFEK) was added to
626 the reverse primer (see Supplemental Table S2 for primer sequences). The pMAL-Tev vector
627 was kindly provided by Alice Barkan. Expression, affinity purification and proteolytic
628 digestion were conducted as described previously (Chi et al., 2014).
629 The EMSA experiments were performed essentially as described previously (Meurer
630 et al., 2017). Increasing concentrations of recombinant RH50 (100 nM, 200 nM, 400 nM)
631 were used.
632
633 **Size exclusion chromatography (SEC)**
634 Size exclusion chromatography of stroma isolated from 3-week-old plants was conducted as
635 described (Meurer et al., 2017). Three milligrams of stroma extracts were used.
636
637 **Accession Numbers**
638 The genes co-expressed with RH50 code for: RH11, DEAD-box ATP-dependent RNA
639 helicase 11 (*At3g58510*); (*At4g01690*); RH17, DEAD-box ATP-dependent RNA helicase 17

(*At2g40700*); RH22, DEAD-box ATP-dependent RNA helicase 22 (*At1g59990*); RH26, DEAD-box ATP-dependent RNA helicase (*At5g08610*); RH52, DEAD-box ATP-dependent RNA helicase 52 (*At3g58570*); RH58, DEAD-box ATP-dependent RNA helicase 58 (*At5g19210*); GUN1, Genomes Uncoupled 1 (*At2g31400*); PRPS1, plastid ribosomal protein S1 (*At5g30510*); CHLD, magnesium chelatase subunit D (*At1g08520*); PPOX, protoporphyrinogen oxidase.

The genes analyzed by Northern blotting, size-exclusion chromatography and polysome fractionation were: *rrn16S* (*AtCg00920*), *rrn23S* (*AtCg01180*), *rrn4.5S* (*AtCg00960*), *rrn5S* (*AtCg00970*), *rbcL* (*AtCg00490*), *psbA* (*AtCg00020*), *LHCA3* (*At1g61520*), *LHCA4* (*At3g47470*), *LHCB1.2* (*At1g29910*), *LHCB4.1* (*At5g01530*), *PSAE1* (*At4g28750*), *PSAK* (*At1g30380*), *PSAO* (*At1g08380*), *PSAD1* (*At4g02770*), *psaA* (*AtCg00350*), *rpl2.1* (*AtCg00830*), *rpl23.1*(*AtCg00840*), *rps8* (*AtCg00770*) and *PRPS3* (*At3g07040*).

The following proteins were analyzed by Y2H: PRPS1, GUN1, CHLD (see above), RH50 (At3g06980), PRPS21 (At3g27160), PRPL11 (At1g32990), PRPL24 (At5g54600), PRPS17(At1g79850).

SUPPLEMENTAL DATA

Supplemental Figure S1. The *rh50-1* mutant is sensitive to cold stress.

Supplemental Figure S2. Characterization of protein interactions of RH50.

Supplemental Figure S3. Polysome loading of the *psaA* mRNA under normal growth conditions.

Supplemental Figure S4. Differential enrichment of chloroplastic RNAs.

Supplemental Table S1. Differentially expressed genes obtained from RNA-seq analysis.

Supplemental Table S2. Primers used in this study.

Acknowledgments

The authors thank Paul Hardy for critical reading of the manuscript.

FIGURES

Figure 1. *RH50* and *GUN1* are co-expressed and their products co-localize in chloroplasts.

A, Co-expression analysis. Among genes coding for chloroplast-localized DBRHs, *RH50* shows the highest co-regulation score with *GUN1*. Correlations between the *GUN1* expression pattern and those of all putative chloroplast-localized DEAD box RNA helicases genes were hierarchically clustered (see Materials and Methods). As a measure of co-expression, *PRPS1,* and *CHLD* and *PPOX* (which encode two enzymes in the tetrapyrrole biosynthesis pathway), which are among the top *GUN1* co-expressors (Tadini et al., 2016), were included. *RH3*, *RH33* and *RH41* are not represented on the Affymetrix array used in our analysis. Degrees of co-expression were measured by the mutual rank (MR) method. Low distance values indicate high co-expression. Full names and accession numbers of corresponding proteins encoded are provided in Materials and Methods. All gene products are predicted or experimentally confirmed chloroplast proteins. **B**, RH50 and GUN1 co-localize in chloroplasts. Protoplasts from 2 weeks-old *Arabidopsis thaliana* cotyledons were isolated (as described in Material and Methods) and co-transfected with GUN1-RFP and RH50-GFP constructs. The RFP signal (red fluorescence) clearly overlapped with the GFP

signal (green fluorescence) within the chloroplast. Fluorescence was imaged by confocal microscopy.

Figure 2. RH50 and regulation of PhANG expression.

A, Schematic representations of the *RH50* mutant alleles. The *rh50-1* and *rh50-2* mutations are due to the insertion of a T-DNA and a transposon, respectively. Left (LB) and right (RB) borders indicate the orientation of the T-DNA, 5' and 3' that of the transposon. Numbered boxes symbolize the exons and black lines the introns. Start and stop codons are indicated. **B**, Immunoblot analysis of total proteins extracted from WT (Col-0 and L*er*), *rh50-1* and *rh50-2* plants was performed with antibodies specific for RH50 (see Materials and Methods) and, as a control, RbcL. **C**, Assay for the *gun* phenotype. RNA gel-blot analysis of *LHCB1.2* expression was carried out using total RNA isolated from wild-type (Col-0) and mutant (*gun1-102*, *rh50-1*, *rh50-1 gun1-102*) seedlings grown for 10 days in the presence of norflurazon (NF) or lincomycin (LIN). **D**, PhANG expression in WT (Col-0) and mutant (*gun1-102*, *rh50-1*, *rh50-1 gun1-102*) plants. Transcripts of nuclear (*LHCA3*, *LHCA4*, *LHCB1*, *LHCB4*, *PSAD1*, *PSAE1*, *PSAO* and *PSAK*) and plastid (*rbcL* and *psbA*) genes encoding photosynthetic functions, isolated from light-adapted WT (Col-0), *rh50-1*, *prors1-1* and *rh50-1 prors1-1* plants, were quantified by RNA gel-blot analysis. Blots were stained with methylene blue (M.B.) to assess RNA loading. Quantification of signals (by ImageJ) relative to Col-0 (=100%) is provided below each panel.

Figure 3. Genetic interactions between *rh50* or *gun1* and mutations (*prors1-1*, *prpl11-1*, *prps1-1*, *prps21-1*, *prps17-1* and *prpl24-1*) affecting PGE.

A, Phenotypes of 26-day-old WT (Col-0 and L*er*), single (*rh50-1*, *rh50-2* and *gun1-102*) mutants and double (*rh50-1 gun1-102*) mutant plants exposed to 80 µmol photons m^{-2} s^{-1}

712 under long-day conditions in a climate chamber. The effective quantum yield of photosystem
713 II (Φ_{II}), measured after a 15-min exposure to actinic light of 37 µmol photons m^{-2} s^{-1} (see
714 Materials and Methods), was determined for each genotype (average ± SD; n ≥ 12). **B**,
715 Growth kinetics of WT (Col-0), *rh50-1*, *gun1-102*, *prpl11-1*, *rh50-1 gun1-102* and *rh50-1*
716 *prpl11-1* were measured at 16, 22 and 26 days after germination (d.a.g.). For each time point,
717 the average leaf area was measured (n ≥ 15). **C**, Phenotypes of single (*prors1-1*, *prpl11-1*,
718 *prps1-1*, *prps21-1*, *rh50-2*, *prps17-1*) and double (*rh50-1 prors1-1*, *gun1-102 prors1-1*, *rh50-*
719 *1 prpl11-1*, *rh50-1 prps1-1*, *gun1-102 prps1-1*, *rh50-1 prps21-1*, *gun1-102 prps21-1*, *rh50-2*
720 *prps17-1*) mutant plants grown and analyzed as in **A**. **D**, Loss of RH50 partially suppresses
721 the reduction in the level of PRPS1 protein seen in the *prps1-1* background. An immunoblot
722 analysis was performed with a PRPS1-specific antibody on extracts of the WT (Col-0), *rh50-*
723 *1* and *prps1-1* single mutants and the *rh50-1 prps1-1* double mutant. To assess loading levels,
724 blots were stained with Coomassie blue, and quantification of signals (by ImageJ) relative to
725 the WT (100%) is provided. **E**, Images of mature embryos (bent cotyledon stage) from WT
726 (Col-0), single (*prpl11-1, prpl24-1, prpl17-1, gun1-102*) and double (*gun1-102 prpl11-1,*
727 *gun1-102 prpl24-1, gun1-102 prpl17-1*) mutant plants. Bars = 200 µm. **F**, Characterization of
728 embryo development in WT (Col-0), single (*rh50-1*, *rh50-2*, *prps24-1*) and double (*rh50-1*
729 *prps24-1, rh50-2 prps24-1*) mutant plants. In 25% of embryos from *RH50/rh50-1 prpl24-*
730 *1/prpl24-1* and *RH50/rh50-2 prpl24-1/prpl24-1* siliques, development ceased at the
731 (disordered) globular stage. Bars = 20 µm.
732
733 **Figure 4. Association of RH50 with chloroplast ribosomes.**
734 **A,** The *rh50-1* mutant is sensitive to erythromycin. Ten-day-old WT (Col-0) and *rh50-1*
735 seedlings were germinated on MS containing 50 µg/mL erythromycin (left panel) or on MS
736 plates without antibiotic (right panel). The maximum quantum yield of photosystem II

737 (F_V/F_M) was determined for each condition (average ± SD; n ≥ 12). The color scale at the
738 bottom indicates the signal intensities. **B**, The *rh50-1* mutant is cold sensitive. Col-0 and
739 *rh50-1* seedlings were germinated at 4°C (left panel) and 22°C (right panel) and transferred
740 to 22°C for 1 week. The maximum quantum yield of photosystem II (F_V/F_M) was determined
741 for each condition (average ± SD; n ≥ 12). The color scale at the bottom indicates the signal
742 intensities. Note that the *rh50-1* mutant phenotype becomes only evident in very young plants
743 (until 1 week after germination as in this panel), whereas after 10 days after germination (as
744 in panel A) the mutant phenotype is recovered. **C**, RH50 co-migrates with ribosomal
745 particles. Following fractionation of RNase-treated and untreated wild-type stromal extracts
746 by size-exclusion chromatography, proteins were precipitated, transferred onto PVDF
747 membranes and immunodecorated with antibodies against RH50, PRPL11 and PRPS5. Note
748 that PRPL11 and PRPS5 accumulate in fractions 3 and 4 when extracts are pretreated with
749 RNase. This might be due to conformational changes induced by partial digestion of the
750 rRNA in mature ribosomes, which makes them less compact, such that they emerge from the
751 column earlier (Jenkins and Barkan, 2001; Meurer et al., 2017). Equal loading is
752 demonstrated by Coomassie Brilliant Blue (C.B.B.) staining of the membrane. Fractions are
753 indicated at the top and complexes were identified on the basis of Olinares et al. (2010).
754 LMW, Low Molecular Weight.
755
756 **Figure 5. RH50 is required for efficient translation in chloroplasts.**
757 **A**, Polysome loading of the *psaA* mRNA. RNA gel-blot analysis of *psaA* transcripts in
758 polysome fractions 1-11 collected after sucrose-gradient centrifugation of cold-treated WT
759 (Col-0) and *rh50-1* extracts. **B**, Pulse-labeling analysis of D1/D2 synthesis. Leaves isolated
760 from plants at the 6-leaf rosette stage were pulse-labeled with [^{35}S]methionine under low-
761 light illumination (20 µmol photons m^{-2} s^{-1}) for 5, 10, and 15 min in the presence of

762 cycloheximide to inhibit cytosolic protein synthesis. Total leaf proteins were then isolated,
763 fractionated by SDS-PAGE and detected by autoradiography. A portion of the SDS-PA gel
764 corresponding to the RbcL region was stained with Coomassie Brilliant Blue (C.B.B.) and
765 served as an internal standard for loading normalization. Quantification of signals (by
766 ImageJ) relative to Col-0 at the 15-min time point (=100%) is provided below each panel.
767
768 **Figure 6. RH50 is required for processing of the *rrn23S-rrn4.5S* rRNA polycistronic**
769 **transcript.**
770 **A**, Transcripts of the *rrn23S-rrn4.5S* intergenic region are enriched in the *rh50-1* mutant. The
771 fold change between *rh50-1* mutant and wild type (Col-0) in read coverage in the 23S and
772 4.5S rRNA genomic region is shown, together with a scale model of the gene. *rrn23S*:
773 position 104690-107500; *rrn4.5S*: 107598-107701. **B**, Schematic representation of the
774 chloroplast rRNA operon in *A. thaliana* showing the locations of the probes (a-e) used for the
775 Northern blot analysis in panel **C**. All precursors, intermediates and mature forms with their
776 respective lengths in kilonucleotides (knt) are shown. The arrows indicate the position of the
777 hidden breaks; white rectangles represent introns. **C**, RNA gel-blot analysis with probes
778 specific for plastid rRNAs (16S, 5S, 23S, 4.5S, 23S-4.5S intergenic region, *rpl2*, *rpl23*, *rps8*,
779 *rps3* and *psbA*) were performed on total RNA isolated from 14-day-old WT (Col-0) and
780 mutant (*gun1-102, rh50-1, gun1-102 rh50-1*) plants.
781
782 **Figure 7. RH50 binds to the *rrn23S-rrn4.5S* intergenic region.**
783 **A,** Western blot analysis of immunoprecipitated RH50. An antibody specific for RH50 (α-
784 RH50) was used, together with the corresponding pre-immune serum (preserum) as a control.
785 p, pellet, sn, supernatant. Note that the lower band (indicated by an asterisk) is a non-specific
786 signal. **B,** Slot-blot analysis of co-immunoprecipitated RNAs. RNAs recovered from the

787 supernatant (sn) and the pellet (p) fractions after immunoprecipitation with α-RH50 or the
788 corresponding pre-immune serum were applied to a nylon membrane using a slot-blot
789 manifold and hybridized with probes specific for the 23S-4.5S intergenic region or *rrn16S* as
790 control. **C**, Affinity purification of MBP-RH50 proteins before and after AcTEV cleavage.
791 Purified proteins were stained with Coomassie Brilliant Blue. **D,** The RNA-binding capacity
792 of the affinity-purified RH50 was analyzed by EMSA using radiolabeled RNA probes for the
793 23 S rRNA and 23 S-4.5S intergenic region as indicated. Increasing concentrations of the
794 purified RH50 protein (black triangles) were used for binding experiments. B; bound, U;
795 unbound.
796

797

Parsed Citations

Amann K, Lezhneva L, Wanner G, Herrmann RG, Meurer J (2004) ACCUMULATION OF PHOTOSYSTEM ONE1, a Member of a Novel Gene Family, Is Required for Accumulation of [4Fe-4S] Cluster–Containing Chloroplast Complexes and Antenna Proteins. Plant Cell 16: 3084

Pubmed: Author and Title
CrossRef: Author and Title
Google Scholar: Author Only Title Only Author and Title

Armbruster U, Zühlke J, Rengstl B, Kreller R, Makarenko E, Rühle T, Schünemann D, Jahns P, Weisshaar B, Nickelsen J, Leister D (2010) The Arabidopsis thylakoid protein PAM68 is required for efficient D1 biogenesis and photosystem II assembly. Plant Cell 22: 3439-3460

Pubmed: Author and Title
CrossRef: Author and Title
Google Scholar: Author Only Title Only Author and Title

Asakura Y, Galarneau E, Watkins KP, Barkan A, van Wijk KJ (2012) Chloroplast RH3 DEAD box RNA helicases in maize and Arabidopsis function in splicing of specific group II introns and affect chloroplast ribosome biogenesis. Plant Physiol 159: 961-974

Pubmed: Author and Title
CrossRef: Author and Title
Google Scholar: Author Only Title Only Author and Title

Barkan A (1993) Nuclear Mutants of Maize with Defects in Chloroplast Polysome Assembly Have Altered Chloroplast RNA Metabolism. Plant Cell 5: 389-402

Pubmed: Author and Title
CrossRef: Author and Title
Google Scholar: Author Only Title Only Author and Title

Bolger AM, Lohse M, Usadel B (2014) Trimmomatic: A flexible trimmer for Illumina sequence data. Bioinformatics 30: 2114-2120

Pubmed: Author and Title
CrossRef: Author and Title
Google Scholar: Author Only Title Only Author and Title

Bollenbach TJ, Lange H, Gutierrez R, Erhardt M, Stern DB, Gagliardi D (2005) RNR1, a 3'-5' exoribonuclease belonging to the RNR superfamily, catalyzes 3' maturation of chloroplast ribosomal RNAs in Arabidopsis thaliana. Nucleic Acids Res 33: 2751-2763

Pubmed: Author and Title
CrossRef: Author and Title
Google Scholar: Author Only Title Only Author and Title

Caruthers JM, McKay DB (2002) Helicase structure and mechanism. Curr Opin Struct Biol 12: 123-133

Pubmed: Author and Title
CrossRef: Author and Title
Google Scholar: Author Only Title Only Author and Title

Chi W, He B, Manavski N, Mao J, Ji D, Lu C, Rochaix JD, Meurer J, Zhang L (2014) RHON1 mediates a Rho-like activity for transcription termination in plastids of Arabidopsis thaliana. Plant Cell 26: 4918-4932

Pubmed: Author and Title
CrossRef: Author and Title
Google Scholar: Author Only Title Only Author and Title

Chi W, He B, Mao J, Li Q, Ma J, Ji D, Zou M, Zhang L (2012) The Function of RH22, a DEAD RNA Helicase, in the Biogenesis of the 50S Ribosomal Subunits of Arabidopsis Chloroplasts. Plant physiol 158: 693-707

Pubmed: Author and Title
CrossRef: Author and Title
Google Scholar: Author Only Title Only Author and Title

Cordin O, Banroques J, Tanner NK, Linder P (2006) The DEAD-box protein family of RNA helicases. Gene 367: 17-37

Pubmed: Author and Title
CrossRef: Author and Title
Google Scholar: Author Only Title Only Author and Title

DalCorso G, Pesaresi P, Masiero S, Aseeva E, Schünemann D, Finazzi G, Joliot P, Barbato R, Leister D (2008) A Complex Containing PGRL1 and PGR5 Is Involved in the Switch between Linear and Cyclic Electron Flow in Arabidopsis. Cell 132: 273-285

Pubmed: Author and Title
CrossRef: Author and Title
Google Scholar: Author Only Title Only Author and Title

Dovzhenko A, Dal Bosco C, Meurer J, Koop HU (2003) Efficient regeneration from cotyledon protoplasts in Arabidopsis thaliana. Protoplasma 222: 107-111

Pubmed: Author and Title
CrossRef: Author and Title
Google Scholar: Author Only Title Only Author and Title

Fristedt R, Scharff LB, Clarke CA, Wang Q, Lin C, Merchant SS, Bock R (2014) RBF1, a plant homolog of the bacterial ribosome-binding

factor RbfA, acts in processing of the chloroplast 16S ribosomal RNA. Plant Physiol 164: 201-215
Pubmed: Author and Title
CrossRef: Author and Title
Google Scholar: Author Only Title Only Author and Title

Giardine B, Riemer C, Hardison RC, Burthans R, Elnitski L, Shah F, Zhang Y, Blankenberg D, Albert I, Taylor J, Miller W, Kent WJ, Nekrutenko A (2005) Galaxy: a platform for interactive large-scale genome analysis. Genome Res 15: 1451-1455
Pubmed: Author and Title
CrossRef: Author and Title
Google Scholar: Author Only Title Only Author and Title

Green MR, Sambrook J (2012) Molecular cloning: a laboratory manual. Cold Spring Harbor Laboratory Press, Cold Spring Harbor, N.Y
Pubmed: Author and Title
CrossRef: Author and Title
Google Scholar: Author Only Title Only Author and Title

Gu L, Xu T, Lee K, Lee KH, Kang H (2014) A chloroplast-localized DEAD-box RNA helicase AtRH3 is essential for intron splicing and plays an important role in the growth and stress response in Arabidopsis thaliana. Plant Physiol Biochem 82: 309-318
Pubmed: Author and Title
CrossRef: Author and Title
Google Scholar: Author Only Title Only Author and Title

Herschlag D (1995) RNA chaperones and the folding problem. J Biol Chem 270: 20871-20874
Pubmed: Author and Title
CrossRef: Author and Title
Google Scholar: Author Only Title Only Author and Title

Huang C-K, Shen Y-L, Huang L-F, Wu S-J, Yeh C-H, Lu C-A (2016) The DEAD-Box RNA Helicase AtRH7/PRH75 Participates in Pre-rRNA Processing, Plant Development and Cold Tolerance in Arabidopsis. Plant Cell Physiol 57: 174-191
Pubmed: Author and Title
CrossRef: Author and Title
Google Scholar: Author Only Title Only Author and Title

Ihnatowicz A, Pesaresi P, Varotto C, Richly E, Schneider A, Jahns P, Salamini F, Leister D (2004) Mutants for photosystem I subunit D of Arabidopsis thaliana: effects on photosynthesis, photosystem I stability and expression of nuclear genes for chloroplast functions. Plant J 37: 839-852
Pubmed: Author and Title
CrossRef: Author and Title
Google Scholar: Author Only Title Only Author and Title

Jarmoskaite I, Russell R (2011) DEAD-box proteins as RNA helicases and chaperones. Wiley Interdiscip Rev RNA 2: 135-152
Pubmed: Author and Title
CrossRef: Author and Title
Google Scholar: Author Only Title Only Author and Title

Jarmoskaite I, Russell R (2014) RNA helicase proteins as chaperones and remodelers. Annu Rev Biochem 83: 697-725
Pubmed: Author and Title
CrossRef: Author and Title
Google Scholar: Author Only Title Only Author and Title

Jenkins BD, Barkan A (2001) Recruitment of a peptidyl-tRNA hydrolase as a facilitator of group II intron splicing in chloroplasts. EMBO J 20: 872-9
Pubmed: Author and Title
CrossRef: Author and Title
Google Scholar: Author Only Title Only Author and Title

Jones PG, Inouye M (1996) RbfA, a 30S ribosomal binding factor, is a cold-shock protein whose absence triggers the cold-shock response. Mol Microbiol 21: 1207-1218
Pubmed: Author and Title
CrossRef: Author and Title
Google Scholar: Author Only Title Only Author and Title

Kaczanowska M, Rydén-Aulin M (2007) Ribosome biogenesis and the translation process in Escherichia coli. Microbiol Mol Biol Rev 71: 477-494
Pubmed: Author and Title
CrossRef: Author and Title
Google Scholar: Author Only Title Only Author and Title

Kant P, Kant S, Gordon M, Shaked R, Barak S (2007) STRESS RESPONSE SUPPRESSOR1 and STRESS RESPONSE SUPPRESSOR2, two DEAD-box RNA helicases that attenuate Arabidopsis responses to multiple abiotic stresses. Plant Physiol 145: 814-830
Pubmed: Author and Title
CrossRef: Author and Title
Google Scholar: Author Only Title Only Author and Title

Kim JS, Kim KA, Oh TR, Park CM, Kang H (2008) Functional Characterization of DEAD-Box RNA Helicases in Arabidopsis thaliana under Abiotic Stress Conditions. Plant Cell Physiol 49: 1563-1571

Pubmed: Author and Title
CrossRef: Author and Title
Google Scholar: Author Only Title Only Author and Title

Kleinknecht L, Wang F, Stübe R, Philippar K, Nickelsen J, Bohne A-V (2014) RAP, the sole octotricopeptide repeat protein in Arabidopsis, is required for chloroplast 16S rRNA maturation. Plant Cell 26: 777-787
Pubmed: Author and Title
CrossRef: Author and Title
Google Scholar: Author Only Title Only Author and Title

Koussevitzky S, Nott A, Mockler TC, Hong F, Sachetto-martins G, Surpin M, Lim J, Mittler R, Chory J (2007) Signals from Chloroplasts Converge to Regulate Nuclear Gene Expression. Science 316: 715–719
Pubmed: Author and Title
CrossRef: Author and Title
Google Scholar: Author Only Title Only Author and Title

Larkin RM, Alonso JM, Ecker JR, Chory J (2003) GUN4, a regulator of chlorophyll synthesis and intracellular signaling. Science 299: 902-906
Pubmed: Author and Title
CrossRef: Author and Title
Google Scholar: Author Only Title Only Author and Title

Li D, Liu H, Zhang H, Wang X, Song F (2008) OsBIRH1, a DEAD-box RNA helicase with functions in modulating defence responses against pathogen infection and oxidative stress. J Exp Bot 59: 2133-2146
Pubmed: Author and Title
CrossRef: Author and Title
Google Scholar: Author Only Title Only Author and Title

Liu HY, Nefsky BS, Walworth NC (2002) The Ded1 DEAD box helicase interacts with Chk1 and Cdc2. J Biol Chem 277: 2637-2643
Pubmed: Author and Title
CrossRef: Author and Title
Google Scholar: Author Only Title Only Author and Title

Liu Y, Tabata D, Imai R (2016) A Cold-Inducible DEAD-Box RNA Helicase from Arabidopsis thaliana Regulates Plant Growth and Development under Low Temperature. PLoS One 11: e0154040-e0154040
Pubmed: Author and Title
CrossRef: Author and Title
Google Scholar: Author Only Title Only Author and Title

Lorsch JR (2002) RNA chaperones exist and DEAD box proteins get a life. Cell 109: 797-800
Pubmed: Author and Title
CrossRef: Author and Title
Google Scholar: Author Only Title Only Author and Title

Love MI, Huber W, Simon A (2014) Moderated estimation of fold change and dispersion for RNA-seq data with DESeq2. Genome Biol 15: 550
Pubmed: Author and Title
CrossRef: Author and Title
Google Scholar: Author Only Title Only Author and Title

Majeran W, Friso G, Asakura Y, Qu X, Huang M, Ponnala L, Watkins KP, Barkan A, van Wijk KJ (2012) Nucleoid-Enriched Proteomes in Developing Plastids and Chloroplasts from Maize Leaves: A New Conceptual Framework for Nucleoid Functions. Plant Physiol 158: 156-189
Pubmed: Author and Title
CrossRef: Author and Title
Google Scholar: Author Only Title Only Author and Title

Meurer J, Schmid L.-S., Stoppel R, Leister D, Brachmann A, Manavski N (2017) PALE CRESS Binds to Plastid RNAs and Facilitates the Biogenesis of the 50S Ribosomal Subunit. Plant J (in press) doi: 10.1111/tpj.13662.
Pubmed: Author and Title
CrossRef: Author and Title
Google Scholar: Author Only Title Only Author and Title

Martinez-Garcia JF, Monte E, Quail PH (1999) A simple, rapid and quantitative method for preparing Arabidopsis protein extracts for immunoblot analysis. Plant J 20: 251-257
Pubmed: Author and Title
CrossRef: Author and Title
Google Scholar: Author Only Title Only Author and Title

Mingam A, Toffano-Nioche C, Brunaud V, Boudet N, Kreis M, Lecharny A (2004) DEAD-box RNA helicases in Arabidopsis thaliana: establishing a link between quantitative expression, gene structure and evolution of a family of genes. Plant Biotechnol J 2: 401-415
Pubmed: Author and Title
CrossRef: Author and Title
Google Scholar: Author Only Title Only Author and Title

Nawaz G, Kang H (2017) Chloroplast- or Mitochondria-Targeted DEAD-Box RNA Helicases Play Essential Roles in Organellar RNA

Metabolism and Abiotic Stress Responses. Front Plant Sci 8: 871
Pubmed: Author and Title
CrossRef: Author and Title
Google Scholar: Author Only Title Only Author and Title

Nishimura K, Ashida H, Ogawa T, Yokota A (2010) A DEAD box protein is required for formation of a hidden break in Arabidopsis chloroplast 23S rRNA. Plant J 63: 766-777
Pubmed: Author and Title
CrossRef: Author and Title
Google Scholar: Author Only Title Only Author and Title

Obayashi T, Hayashi S, Saeki M, Ohta H, Kinoshita K (2009) ATTED-II provides coexpressed gene networks for Arabidopsis. Nucleic Acids Res 37: D987-991
Pubmed: Author and Title
CrossRef: Author and Title
Google Scholar: Author Only Title Only Author and Title

Obayashi T, Kinoshita K, Nakai K, Shibaoka M, Hayashi S, Saeki M, Shibata D, Saito K, Ohta H (2007) ATTED-II: a database of co-expressed genes and cis elements for identifying co-regulated gene groups in Arabidopsis. Nucleic Acids Res 35: D863-869
Pubmed: Author and Title
CrossRef: Author and Title
Google Scholar: Author Only Title Only Author and Title

Olinares PD, Ponnala L, van Wijk KJ (2010) Megadalton complexes in the chloroplast stroma of Arabidopsis thaliana characterized by size exclusion chromatography, mass spectrometry, and hierarchical clustering. Mol Cell Proteomics 9: 1594-1615
Pubmed: Author and Title
CrossRef: Author and Title
Google Scholar: Author Only Title Only Author and Title

Owttrim GW (2006) RNA helicases and abiotic stress. Nucleic Acids Res 34: 3220-3230
Pubmed: Author and Title
CrossRef: Author and Title
Google Scholar: Author Only Title Only Author and Title

Pesaresi P, Hertle A, Pribil M, Kleine T, Wagner R, Strissel H, Ihnatowicz A, Bonardi V, Scharfenberg M, Schneider A, Pfannschmidt T, Leister D (2009) Arabidopsis STN7 kinase provides a link between short- and long-term photosynthetic acclimation. Plant Cell 21: 2402-23
Pubmed: Author and Title
CrossRef: Author and Title
Google Scholar: Author Only Title Only Author and Title

Pesaresi P, Masiero S, Eubel H, Braun H-P, Bhushan S, Glaser E, Salamini F, Leister D (2006) Nuclear photosynthetic gene expression is synergistically modulated by rates of protein synthesis in chloroplasts and mitochondria. Plant Cell 18: 970-991
Pubmed: Author and Title
CrossRef: Author and Title
Google Scholar: Author Only Title Only Author and Title

Pesaresi P, Varotto C, Meurer J, Jahns P, Salamini F, Leister D (2001) Knock-out of the plastid ribosomal protein L11 in Arabidopsis: effects on mRNA translation and photosynthesis. Plant J 27: 179-189
Pubmed: Author and Title
CrossRef: Author and Title
Google Scholar: Author Only Title Only Author and Title

Rogalski M, Schöttler MA, Thiele W, Schulze WX, Bock R (2008) Rpl33, a Nonessential Plastid-Encoded Ribosomal Protein in Tobacco, Is Required under Cold Stress Conditions. Plant Cell 20: 2221-37
Pubmed: Author and Title
CrossRef: Author and Title
Google Scholar: Author Only Title Only Author and Title

Romani I, Tadini L, Rossi F, Masiero S, Pribil M, Jahns P, Kater M, Leister D, Pesaresi P (2012) Versatile roles of Arabidopsis plastid ribosomal proteins in plant growth and development. Plant J 72: 922-34
Pubmed: Author and Title
CrossRef: Author and Title
Google Scholar: Author Only Title Only Author and Title

Rosso MG, Li Y, Strizhov N, Reiss B, Dekker K, Weisshaar B (2003) An Arabidopsis thaliana T-DNA mutagenized population (GABI-Kat) for flanking sequence tag-based reverse genetics. Plant Mol Biol 53: 247-259
Pubmed: Author and Title
CrossRef: Author and Title
Google Scholar: Author Only Title Only Author and Title

Shajani Z, Sykes MT, Williamson JR (2011) Assembly of bacterial ribosomes. Annu Rev Biochem 80: 501-526
Pubmed: Author and Title
CrossRef: Author and Title
Google Scholar: Author Only Title Only Author and Title

Romani I, Tadini L, Rossi F, Masiero S, Pribil M, Jahns P, Kater M, Leister D, Pesaresi P (2012) Versatile roles of Arabidopsis plastid ribosomal proteins in plant growth and development. Plant J 72: 922-934
Pubmed: Author and Title
CrossRef: Author and Title
Google Scholar: Author Only Title Only Author and Title

Silverman E, Edwalds-Gilbert G, Lin R-J (2003) DExD/H-box proteins and their partners: helping RNA helicases unwind. Gene 312: 1-16
Pubmed: Author and Title
CrossRef: Author and Title
Google Scholar: Author Only Title Only Author and Title

Sohmen D, Harms JM, Schlünzen F, Wilson DN (2009) SnapShot: Antibiotic inhibition of protein synthesis I. Cell 138: 1248.e1.
Pubmed: Author and Title
CrossRef: Author and Title
Google Scholar: Author Only Title Only Author and Title

Stoppel R, Lezhneva L, Schwenkert S, Torabi S, Felder S, Meierhoff K, Westhoff P, Meurer J (2011) Recruitment of a ribosomal release factor for light- and stress-dependent regulation of petB transcript stability in Arabidopsis chloroplasts. Plant Cell 23: 2680-95
Pubmed: Author and Title
CrossRef: Author and Title
Google Scholar: Author Only Title Only Author and Title

Stoppel R, Manavski N, Schein A, Schuster G, Teubner M, Schmitz-Linneweber C, Meurer J (2012) RHON1 is a novel ribonucleic acid-binding protein that supports RNase e function in the Arabidopsis chloroplast. Nucleic Acids Res 40: 8593-8606
Pubmed: Author and Title
CrossRef: Author and Title
Google Scholar: Author Only Title Only Author and Title

Sun X, Xu D, Liu Z, Kleine T, Leister D (2016) Functional relationship between mTERF4 and GUN1 in retrograde signaling. J Exp Bot 67: 3909-3924
Pubmed: Author and Title
CrossRef: Author and Title
Google Scholar: Author Only Title Only Author and Title

Tadini L, Pesaresi P, Kleine T, Rossi F, Guljamow A, Sommer F, Mühlhaus T, Schroda M, Masiero S, Pribil M, Rothbart M, Hedtke B, Grimm B, Leister D (2016) GUN1 Controls Accumulation of the Plastid Ribosomal Protein S1 at the Protein Level and Interacts with Proteins Involved in Plastid Protein Homeostasis. Plant Physiol 170: 1817-1830
Pubmed: Author and Title
CrossRef: Author and Title
Google Scholar: Author Only Title Only Author and Title

Vashisht AA, Tuteja N (2006) Stress responsive DEAD-box helicases: A new pathway to engineer plant stress tolerance. J Photochem Photobiol B 84: 150-160
Pubmed: Author and Title
CrossRef: Author and Title
Google Scholar: Author Only Title Only Author and Title

Vinti G, Hills A, Campbell S, Bowyer JR, Mochizuki N, Chory J, López-Juez E (2000) Interactions between hy1 and gun mutants of Arabidopsis, and their implications for plastid/nuclear signaling. Plant J 24: 883-894
Pubmed: Author and Title
CrossRef: Author and Title
Google Scholar: Author Only Title Only Author and Title

Wang S, Bai G, Wang S, Yang L, Yang F, Wang Y, Zhu J-K, Hua J (2016) Chloroplast RNA-Binding Protein RBD1 Promotes Chilling Tolerance through 23S rRNA Processing in Arabidopsis. PLoS Genet 12: e1006027
Pubmed: Author and Title
CrossRef: Author and Title
Google Scholar: Author Only Title Only Author and Title

Wang Y, Duby G, Purnelle B, Boutry M (2000) Tobacco VDL gene encodes a plastid DEAD box RNA helicase and is involved in chloroplast differentiation and plant morphogenesis. Plant Cell 12: 2129-2142
Pubmed: Author and Title
CrossRef: Author and Title
Google Scholar: Author Only Title Only Author and Title

Wu W, Liu S, Ruwe H, Zhang D, Melonek J, Zhu Y, Hu X, Gusewski S, Yin P, Small ID, Howell KA, Huang J (2016) SOT1, a pentatricopeptide repeat protein with a small MutS-related domain, is required for correct processing of plastid 23S-4.5S rRNA precursors in Arabidopsis thaliana. Plant J 85: 607-621
Pubmed: Author and Title
CrossRef: Author and Title
Google Scholar: Author Only Title Only Author and Title

Yin T, Pan G, Liu H, Wu J, Li Y, Zhao Z, Fu T, Zhou Y (2012) The chloroplast ribosomal protein L21 gene is essential for plastid development and embryogenesis in Arabidopsis. Planta 235: 907-921
Pubmed: Author and Title

Zhang J, Yuan H, Yang Y, Fish T, Lyi SM, Thannhauser TW, Zhang L, Li L (2016) Plastid ribosomal protein S5 is involved in photosynthesis, plant development, and cold stress tolerance in Arabidopsis. J Exp Bot 67: 2731-2744